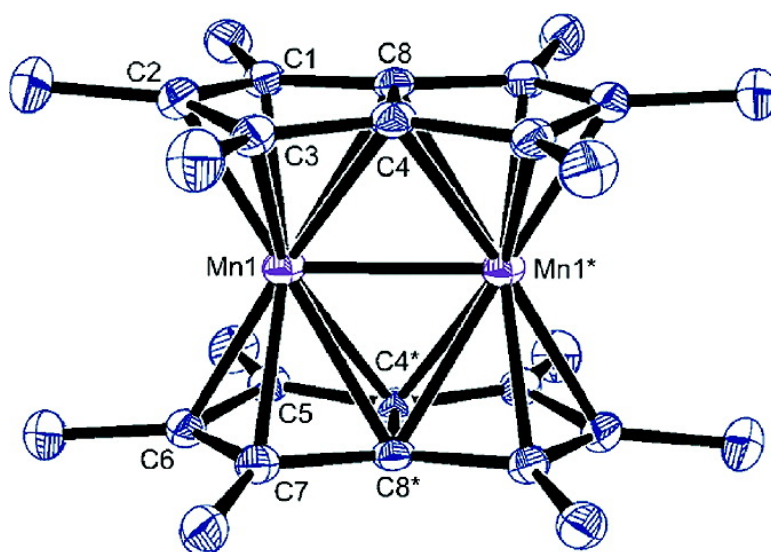Article

Homoleptic Permethylpentalene Complexes: "Double Metallocenes" of the First-Row Transition Metals

Andrew E. Ashley, Robert T. Cooper, Gregory G. Wildgoose, Jennifer C. Green, and Dermot O'Hare

More About This Article

Additional resources and features associated with this article are available within the HTML version:

- Supporting Information
- Access to high resolution figures
- Links to articles and content related to this article
- Copyright permission to reproduce figures and/or text from this article

View the Full Text HTML

Homoleptic Permethylpentalene Complexes: "Double Metallocenes" of the First-Row Transition Metals

Andrew E. Ashley,[†] Robert T. Cooper,[†] Gregory G. Wildgoose,[‡] Jennifer C. Green,[*,§] and Dermot O'Hare[*,†]

Chemistry Research Laboratory, Oxford University, Mansfield Rd, Oxford OX1 3TA, U.K., Physical and Theoretical Chemistry Laboratory, Oxford University, South Parks Rd, Oxford OX1 3QZ, U.K., and Inorganic Chemistry Laboratory, Oxford University, South Parks Rd, Oxford OX1 3QR, U.K.

Received July 22, 2008; E-mail: jennifer.green@chem.ox.ac.uk; dermot.ohare@chem.ox.ac.uk

Abstract: The synthesis of the bimetallic permethylpentalene complexes $Pn^*_2M_2$ (M = V, Cr, Mn, Co, Ni; $Pn^* = C_8Me_6$) has been accomplished, and all of the complexes have been structurally characterized in the solid state by single-crystal X-ray diffraction. $Pn^*_2V_2$ (**1**) and $Pn^*_2Mn_2$ (**3**) show very short intermetallic distances that are consistent with metal−metal bonding, while the cobalt centers in $Pn^*_2Co_2$ (**4**) exhibit differential bonding to each side of the Pn^* ligand that is consistent with an $\eta^5:\eta^3$ formulation. The Pn^* ligands in $Pn^*_2Ni_2$ (**5**) are best described as $\eta^3:\eta^3$-bonded to the metal centers. ^1H NMR studies indicate that all of the $Pn^*_2M_2$ species exhibit D_{2h} molecular symmetry in the solution phase; the temperature variation of the chemical shifts for the resonances of $Pn^*_2Cr_2$ (**2**) indicates that the molecule has an $S = 0$ ground state and a thermally populated $S = 1$ excited state and can be successfully modeled using a Boltzmann distribution ($\Delta H^\circ = 14.9$ kJ mol^{-1} and $\Delta S^\circ = 26.5$ J K^{-1} mol^{-1}). The solid-state molar magnetic susceptibility of **3** obeys the Curie−Weiss law with $\mu_{eff} = 2.78\mu_B$ and $\theta = -1.0$ K; the complex is best described as having an $S = 1$ electronic ground state over the temperature range 4−300 K. Paradoxically, attempts to isolate the "double ferrocene" equivalent, $Pn^*_2Fe_2$, led only to the isolation of the permethylpentalene dimer Pn^*_2 (**6**). Solution electrochemical studies were performed on all of the organometallic compounds; **2−5** exhibit multiple quasi-reversible redox processes. Density functional theory calculations were performed on this series of complexes in order to rationalize the observed structural and spectroscopic data and provide estimates of the M−M bond orders.

Introduction

Over the past 30 years, numerous spectroscopic studies have enabled chemists to develop a detailed understanding of the electronic structure and bonding in bis(cyclopentadienyl) "sandwich" complexes of the first-row transition metals. These efforts were spawned by the structural elucidation of Cp_2Fe, arguably the starting point for the birth of modern organometallic chemistry.[1] The intriguing redox, electronic, and magnetic properties that these complexes exhibit have lent themselves to myriad diverse applications in catalysis and materials chemistry. For instance, the decamethylmetallocenium (Cp^*_2M; M = Cr, Mn, Fe) charge-transfer salts with organic acceptors (TCNQ, TCNE, and DDQ derivatives) have demonstrated behavior normally associated with the metallic phase, such as bulk ferromagnetic ordering, and thus provided prototypes for mole-cular-based ferromagnets.[2] Cobaltocene and its methylated derivatives have been used as electronic dopants through redox intercalation within lamellar lattices (e.g., TaS_2, $SnSe_2$, and β-$ZrNCl$), with the resultant materials displaying superconductivity.[3] Ferrocenes, because of their stability, availability, and substitutional flexibility, have found extensive use in the production of second- and third-order nonlinear optical materials,[4] in ferrocenyl-based polymers displaying electrical conduction and useful mechanical properties,[5] as redox-active chemical sensors in functionalized macrocyclic frameworks,[6] and as chiral

† Chemistry Research Laboratory.
‡ Physical and Theoretical Chemistry Laboratory.
§ Inorganic Chemistry Laboratory.

(1) (a) Long, N. J. *Metallocenes: An Introduction to Sandwich Complexes*; Blackwell Science: Oxford, U.K., 1998. (b) *Metallocenes*; Togni, A.; Halterman, R. L., Eds.; Wiley-VCH: Weinheim, Germany, 1998. (c) Haaland, A. *Acc. Chem. Res.* **1979**, *12*, 415–422. (d) Hays, M. L.; Hanusa, T. P. *Adv. Organomet. Chem.* **1996**, *40*, 117–170. (e) Gruhn, N. E.; Lichtenberger, D. L. *Inorg. Electron. Struct. Spectrosc.* **1999**, *2*, 533–574.

(2) (a) Yee, G. T.; Manriquez, J. M.; Dixon, D. A.; Mclean, R. S.; Groski, D. M.; Flippen, R. B.; Narayan, K. S.; Epstein, A. J.; Miller, J. S. *Adv. Mater.* **1991**, *3*, 309–311. (b) Miller, J. S.; Vazquez, C.; Mclean, R. S.; Reiff, W. M.; Aumueller, A.; Huenig, S. *Adv. Mater.* **1993**, *5*, 448–450. (c) Wang, G.; Slebodnick, C.; Butcher, R. J.; Tam, M. C.; Crawford, T. D.; Yee, G. T. *J. Am. Chem. Soc.* **2004**, *126*, 16890–16895. (d) Miller, J. S.; Epstein, A. J. *Angew. Chem., Int. Ed. Engl.* **1994**, *33*, 385–415. (e) Miller, J. S.; Epstein, A. J.; Reiff, W. M. *Science* **1988**, *240*, 40–47. (f) Manriquez, J. M.; Yee, G. T.; Mclean, R. S.; Epstein, A. J.; Miller, J. S. *Science* **1991**, *252*, 1415–1417. (g) Miller, J. S. *Dalton Trans.* **2006**, 2742–2749.

(3) (a) Fogg, A. M.; Green, V. M.; O'Hare, D. *Chem. Mater.* **1999**, *11*, 216–217. (b) O'Hare, D.; Evans, J. S. O. *Comments Inorg. Chem.* **1993**, *14*, 155–206. (c) Wong, H.-V.; Evans, J. S. O.; Barlow, S.; Mason, S. J.; O'Hare, D. *Inorg. Chem.* **1994**, *33*, 5515–5521. (d) Evans, J. S. O.; O'Hare, D.; Clement, R. *J. Am. Chem. Soc.* **1995**, *117*, 4595–4606. (e) Bruce, D. B.; O'Hare, D. *Inorganic Materials*, 2nd ed.; Wiley: Chichester, U.K., 1996.

ligand auxiliaries for use in asymmetric catalysis.[7] Furthermore, the use of metallocenes is not just restricted to the world of materials; water-soluble ferrocenium and cobaltocenium salts have shown promising cytotoxicities against cancer cells, and it is anticipated that new biomedical applications for such species will rapidly emerge.[8]

Pentalene (Pn, C_8H_6), as the double ring-fused relative of the ubiquitous Cp ligand, could be envisaged to encapsulate metal centers between two ligand planes, thus providing bimetallic analogues of the metallocenes.[9] Katz, the pioneer of organometallic pentalene chemistry, synthesized the first pentalene-based sandwich complexes Pn_2M_2 (M = Co, Ni) and observed their diamagnetism to be in contrast with the behavior of their bis(cyclopentadienyl) counterparts; unfortunately no crystallographic evidence has subsequently been provided to establish whether M−M bonding or superexchange through the ligand π system is responsible for the spin pairing.[10,11] Some years later, Cloke and co-workers documented the complexes $(\mu:\eta^5,\eta^5\text{-}C_8H_4^{1,4\text{-}iPr_3Si})_2M_2$ (M = Cr, Mo, Mn, Rh, Pd), with the first row species only very recently appearing in the literature.[12−15] However, a comprehensive treatment of such a series of compounds *across* a period is lacking. In recent years, organometallic Pn chemistry has seen resurgence in activity as a result of the development of facile syntheses of new silyl- and alkyl-substituted Pn derivatives.[16,17] We recently reported the syn-

thesis of the permethylpentalene (Pn*, C_8Me_6) derivatives $Li_2Pn*(TMEDA)_x$ and $Pn*(SnMe_3)_2$;[18,19] in this paper, we report the application of these reagents to the synthesis and detailed characterization of a systematic range of transition-metal "double metallocenes" $Pn*_2M_2$ (M = V, Cr, Mn, Co, Ni), which show structural, magnetic, and electrochemical behavior that is markedly different than that found for their mononuclear cyclopentadienyl analogues.

Experimental Section

General Comments. All of the manipulations were performed under an inert atmosphere of nitrogen gas, utilizing standard Schlenk techniques on a dual-vacuum-inlet gas manifold or MBraun UNIlab glovebox. Each solvent was purified either by reflux over sodium benzophenone diketyl (THF) or passage through activated alumina (pentane, hexane, toluene, Et_2O, DME) using an MBraun SPS-800 solvent system. All of the solvents were thoroughly degassed by passage of a stream of inert gas. Toluene-d_8 was freeze−pump−thaw-degassed, dried by reflux over molten K, and purified by trap-to-trap distillation. The following instrumentation was used: Varian Unity Plus 500 MHz or Varian Mercury VX-Works 300 MHz spectrometer for ^1H and ^{13}C spectroscopy (recorded at 300 K unless otherwise stated); PerkinElmer Paragon 1000 FT-IR spectrometer for IR spectroscopy; SCINCO UV S-2100 spectrometer for UV spectroscopy; and Waters GCT with an EI source for mass spectrometry. Elemental microanalyses were conducted by Stephen Boyer at London Metropolitan University.

X-ray crystallographic data were collected on an Enraf-Nonius FR590 KappaCCD diffractometer; the structures were solved by direct methods (SIR92) and refined (on F^2) by full-matrix least-squares (CRYSTALS).

Solid-state magnetic susceptibility data were obtained using a Quantum Design MPMS-5 SQUID magnetometer. Accurately weighed samples (~0.040 g) were placed into gelatin capsules and then loaded into nonmagnetic plastic straws before being lowered into the cryostat. The field independence of the measurement was verified by measuring the susceptibility as a function of field between −5 and 5 T. Data were then collected employing a field of 0.1 T and finally corrected for the inherent diamagnetism of the sample by use of Pascal's constants.[20]

X-band continuous-wave EPR measurements were made on a Bruker EMX spectrometer equipped with an Elexsys super high sensitivity probe head and an Oxford continuous-flow cryostat (ESR900). All of the measurements employed a modulation frequency of 100 kHz. For **2**, spectra were recorded at 9.390 and 9.380 GHz with modulation amplitudes of 0.10 and 0.50 mT and microwave powers of 20 and 63 mW at 293 and 90 K, respectively, whereas for **3**, spectra were recorded at 9.382 and 9.380 GHz with modulation amplitudes of 0.50 and 0.25 mT and microwave powers of 2.0 and 6.3 mW at 293 and 7.4 K, respectively.

Electrochemical experiments were performed in dry THF containing 0.1 M $[^nBu_4][NBF_4]$ as the supporting electrolyte using an Autolab PGStat 20 computer-controlled potentiostat (EcoChemie, Utrecht, The Netherlands). Cyclic voltammetry experiments were performed using a three-electrode configuration with a Pt macrodisc electrode (99.99%, Goodfellow, Huntingdon, U.K.) having an area of $(1.4 \pm 0.2) \times 10^{-3}$ cm^2 as the working electrode, a Pt gauze as the counter electrode, and a Ag wire as the pseudoreference electrode. The Ag wire pseudoreference electrode was calibrated to the ferrocene/ferrocenium couple in THF, relative to which all of the standard potentials are reported. A scan rate of 100 mV s^{-1} was used in all of the cyclic voltammetry experiments, unless stated otherwise. Chronoamperometry was recorded using a Pt micro-

(4) (a) Long, N. J. *Angew. Chem., Int. Ed. Engl.* **1995**, *34*, 21–38. (b) Braga, D.; Grepioni, F.; Desiraju, G. R. *Chem. Rev.* **1998**, *98*, 1375–1405. (c) Whittall, I. R.; Mcdonagh, A. M.; Humphrey, M. G.; Samoc, M. *Adv. Organomet. Chem.* **1998**, *42*, 291–362. (d) Di Bella, S. *Chem. Soc. Rev.* **2001**, *30*, 355–366. (e) Peris, E. *Coord. Chem. Rev.* **2004**, *248*, 279–297. (f) Asselberghs, I.; Clays, K.; Persoons, A.; Ward, M. D.; McCleverty, J. *J. Mater. Chem.* **2004**, *14*, 2831–2839.

(5) (a) Barlow, S.; O'Hare, D. *Chem. Rev.* **1997**, *97*, 637–669. (b) Herbert, D. E.; Mayer, U. F. J.; Manners, I. *Angew. Chem., Int. Ed.* **2007**, *46*, 5060–5081. (c) Nguyen, P.; Gomez-Elipe, P.; Manners, I. *Chem. Rev.* **1999**, *99*, 1515–1548.

(6) (a) Nijhuis, C. A.; Ravoo, B. J.; Huskens, J.; Reinhoudt, D. N. *Coord. Chem. Rev.* **2007**, *251*, 1761–1780. (b) Constable, E. C. *Angew. Chem., Int. Ed. Engl.* **1991**, *30*, 407–408. (c) Siemeling, U. *Z. Anorg. Allg. Chem.* **2005**, *631*, 2957–2966. (d) Beer, P. D. *Adv. Inorg. Chem.* **1992**, *39*, 79–157.

(7) (a) Dai, L.-X.; Tu, T.; You, S.-L.; Deng, W.-P.; Hou, X.-L. *Acc. Chem. Res.* **2003**, *36*, 659–667. (b) Atkinson, R. C. J.; Gibson, V. C.; Long, N. J. *Chem. Soc. Rev.* **2004**, *33*, 313–328. (c) Barbaro, P.; Bianchini, C.; Giambastiani, G.; Parisel, S. L. *Coord. Chem. Rev.* **2004**, *248*, 2131–2150. (d) Gomez Arrayas, R.; Adrio, J.; Carretero, J. C. *Angew. Chem., Int. Ed.* **2006**, *45*, 7674–7715.

(8) (a) Dombrowski, K. E.; Baldwin, W.; Sheats, J. E. *J. Organomet. Chem.* **1986**, *302*, 281–306. (b) Guo, Z.; Sadler, P. J. *Adv. Inorg. Chem.* **2000**, *49*, 183–306. (c) Van Staveren, D. R.; Metzler-Nolte, N. *Chem. Rev.* **2004**, *104*, 5931–5985. (d) Fouda, M. F. R.; Abd-Elzaher, M. M.; Abdelsamaia, R. A.; Labib, A. A. *Appl. Organomet. Chem.* **2007**, *21*, 613–625. (e) Jaouen, G.; Top, S.; Vessieres, A. *Bioorganometallics* **2006**, 65–95.

(9) (a) Knox, S. A. R.; Stone, F. G. A. *Acc. Chem. Res.* **1974**, *7*, 321–328. (b) Butenschon, H. *Angew. Chem., Int. Ed. Engl.* **1997**, *36*, 1695–1697. (c) Summerscales, O. T.; Cloke, F. G. N. *Coord. Chem. Rev.* **2006**, *250*, 1122–1140.

(10) Katz, T. J.; Acton, N. *J. Am. Chem. Soc.* **1972**, *94*, 3281–3283.

(11) Katz, T. J.; Acton, N.; McGinnis, J. *J. Am. Chem. Soc.* **1972**, *94*, 6205–6206.

(12) Kuchta, M. C.; Cloke, F. G. N.; Hitchcock, P. B. *Organometallics* **1998**, *17*, 1934–1936.

(13) Cloke, F. G. N. *Pure Appl. Chem.* **2001**, *73*, 233–238.

(14) Balazs, G.; Cloke, F. G. N.; Harrison, A.; Hitchcock, P. B.; Green, J.; Summerscales, O. T. *Chem. Commun.* **2007**, 873–875.

(15) Balazs, G.; Cloke, F. G. N.; Gagliardi, L.; Green, J. C.; Harrison, A.; Hitchcock, P. B.; Shahi, A. R. M.; Summerscales, O. T. *Organometallics* **2008**, *27*, 2013–2020.

(16) Cloke, F. G. N.; Kuchta, M. C.; Harker, R. M.; Hitchcock, P. B.; Parry, J. S. *Organometallics* **2000**, *19*, 5795–5798.

(17) Jones, S. C.; Roussel, P.; Hascall, T.; O'Hare, D. *Organometallics* **2006**, *25*, 221–229.

(18) Ashley, A. E.; Cowley, A. R.; O'Hare, D. *Chem. Commun.* **2007**, 1512–1514.

(19) Ashley, A. E.; Cowley, A. R.; O'Hare, D. *Eur. J. Org. Chem.* **2007**, 2239–2242.

(20) O'Connor, C. J. *Prog. Inorg. Chem.* **1982**, *29*, 203–283.

electrode (99.99%, Goodfellow) having a radius of 4.5 ± 0.5 μm in a standard two-electrode configuration in a specially designed T-cell with a Ag wire pseudoreference electrode.[21] All of the electrochemical experiments were performed under an inert nitrogen atmosphere. The Pt working electrodes were polished using alumina slurries of decreasing particle size (1.0−0.3 μm, Buehler, Lake Bluff, IL). After each successive polishing, the electrodes were briefly sonicated in ethanol to remove any adhered microparticles and allowed to dry thoroughly; upon completion of the polishing process, the electrodes were immersed in the dry THF electrolyte under a nitrogen atmosphere. The areas of the Pt microdisc and macrodisc working electrodes were calibrated using 1.0 mM $K_3[Fe(CN)_6]$ in 0.1 M KCl aqueous electrolyte prior to use. $CrCl_2$ and $MnCl_2$ were purchased from Strem and all of the other chemicals from Aldrich; all were used as received. Li_2Pn^*-$(TMEDA)_x$ (x = 0.12),[18] *cis*-$Pn^*(SnMe_3)_2$,[18] $VCl_2(DME)$,[22] $FeCl_2(THF)_{1.5}$,[23] $CoBr_2(DME)$,[24] and $NiCl_2(DME)$[25] were prepared according to literature procedures.

Quantum-chemical calculations were performed using density functional theory (DFT) methods as implemented in the Amsterdam Density Functional package (version ADF2007.01).[26] In these calculations, the generalized gradient approximation was employed using the local density approximation of Vosko, Wilk, and Nusair[27] together with the nonlocal-exchange correction by Becke[28] and the nonlocal-correlation corrections by Perdew.[29] TZP basis sets with triple-ξ-accuracy sets of Slater-type orbitals and with polarization functions added to all of the atoms were used. Relativistic corrections were made using the zero-order relativistic approximation formalism. The core electrons (up to 1s for carbon and 2p for the transition metals) were frozen. The geometries were optimized with and without symmetry constraints and with spin states $S = 0$ and 1, except for Mn, where larger values of S were also employed. Fragment analyses on the D_{2h} $S = 0$ structures afforded a decomposition of the bonding in terms of the molecular orbitals (MOs) of the M_2 dimer and the Pn^* ligands and enabled an estimation of the M−M bond order.[30]

$Pn^*_2V_2$ (1). $Li_2Pn^*(TMEDA)_{0.12}$ (1.00 g, 4.67 mmol) in THF (20 mL) was added to a slurry of $VCl_2 \cdot DME$ (0.99 g, 4.67 mmol) in THF (20 mL) while stirring at −78 °C. The mixture was allowed to stir for 1 h at −40 °C before it was warmed to room temperature, during which time the solution turned orange-brown. After 24 h, the THF was removed under reduced pressure and the residue subjected to dynamic vacuum (10^{-3} mbar) for 24 h. The resultant solid was then ground, transferred to a sublimator, and sublimed at 120−130 °C under high vacuum (10^{-6} mbar) to produce a bright-red powder (*very air-sensitive*) that was washed with cold (−78 °C) pentane and dried under vacuum. Yield: 7.0% (0.078 g, 0.16 mmol); Anal. Found (Calcd) for $C_{28}H_{36}V_2$: C, 70.96 (70.88); H, 7.58 (7.65). ^1H NMR (C_7D_8, 300 MHz): δ 2.10 (s, 24H, CH_3), 0.87 (s, 12H, CH_3). $^{13}C\{^1H\}$ NMR (C_7D_8, 75 MHz): δ 97.4 (s, ring-C), 86.5 (s, ring-C), 74.1 (s, ring-C), 12.2 (s, 2 × CH_3). IR (KBr, cm^{-1}): 2952, 2929, 2903, 2852 (all s, ν_{CH}), 1456 (m, $\nu_{C=C}$), 1379 (s), 1261 (m), 1196 (w), 1093 (m), 1020 (s), 799 (m). HRMS (EI): *m/z* calcd for $C_{28}H_{36}V_2$ (M), 474.1696; found, 474.1683. UV

λ_{max} (ε_{max}): 546 (1080), 417 (2030), 370 (2350), 309 (11860), 252 (17640), 237 (14920).

$Pn^*_2Cr_2$ (2). $CrCl_2$ (0.57 g, 4.65 mmol) in THF (20 mL) was heated to 55 °C and stirred for 24 h. $Li_2Pn^*(TMEDA)_{0.12}$ (1.00 g, 4.67 mmol) in THF (20 mL) was then added to the suspension at −78 °C and stirred for 1 h, after which time the mixture had turned green. The mixture was then slowly allowed to warm to room temperature, during which time the mixture became homogeneous. The solvent was stripped in vacuo to yield a dark solid, which was subjected to dynamic vacuum (10^{-3} mbar) for 24 h. The resulting material was transferred to a Soxhlet apparatus and extracted with toluene (125 mL) over 2 days. The dark-green solution was subsequently cooled to −35 °C, producing emerald-green microcrystals that were washed with cold THF (−78 °C) and dried under vacuum. Yield: 48.8% (0.543 g, 1.14 mmol). Anal. Found (Calcd) for $C_{28}H_{36}Cr_2$: C, 70.50 (70.57); H, 7.49 (7.61). ^1H NMR (C_7D_8, 300 MHz, 303 K): δ 8.97 (br, 12H, $\Delta\nu_{1/2}$ = 80 Hz, CH_3), 2.04 (s, 24H, CH_3). IR (KBr, cm^{-1}): 2957, 2936, 2903, 2854 (all s, ν_{CH}), 1449 (m, $\nu_{C=C}$), 1378 (s), 1260 (m), 1188 (w), 1092 (m), 1025 (s), 801 (m). HRMS (EI): *m/z* calcd for $C_{28}H_{36}Cr_2$ (M), 476.1627; found, 474.1619. UV λ_{max} (ε_{max}): 443 (2510), 416 (3390), 319 (7600), 248 (21000).

$Pn^*_2Mn_2$ (3). $MnCl_2$ (0.58 g, 4.67 mmol) was stirred in THF (30 mL) at room temperature for 24 h to form $MnCl_2(THF)_{1.5}$. $Li_2Pn^*(TMEDA)_{0.12}$ (1.00 g, 4.67 mmol) in THF (20 mL) was then added while stirring at −78 °C, and the mixture was allowed to warm to ambient temperature, during which time the solution turned green in color. The volatiles were removed under reduced pressure and the residue subjected to dynamic vacuum (10^{-3} mbar) for 24 h. The solid was then extracted with hexane (150 mL) using a Soxhlet apparatus to produce microcrystalline **3** (*extremely air-sensitive*) after cooling to room temperature; the product was washed with cold toluene (−78 °C) and dried in vacuo. Yield: 21.1% (0.238 g, 0.49 mmol). Anal. Found (Calcd) for $C_{28}H_{36}Mn_2$: C, 69.64 (69.71); H, 7.50 (7.52). ^1H NMR (C_7D_8, 300 MHz): δ 59.76 (br, 12H, $\Delta\nu_{1/2}$ = 766 Hz, CH_3), −19.15 (br, 24H, $\Delta\nu_{1/2}$ = 918 Hz, CH_3). IR (KBr, cm^{-1}): 2961, 2937, 2907, 2854 (all s, ν_{CH}), 1445 (m, $\nu_{C=C}$), 1376 (s), 1261 (m), 1094 (m), 1022 (s), 801 (m). HRMS (EI): *m/z* calcd for $C_{28}H_{36}Mn_2$ (M), 482.1578; found, 482.1578. UV λ_{max} (ε_{max}): 348 (1020), 308 (3440), 268 (5480), 224 (7760).

$Pn^*_2Co_2$ (4). THF (40 mL) was added to a mixture of $CoBr_2$-(DME) (0.60 g, 1.95 mmol) and *cis*-$Pn^*(SnMe_3)_2$ (1.00 g, 1.95 mmol) while stirring at room temperature, and the slurry rapidly turned green. After an additional 24 h, the solution was filtered through Celite on a sintered frit, and the solvent was stripped in vacuo to give a solid that was washed with pentane (2 × 20 mL). The remaining material was extracted with toluene (60 °C, 3 × 30 mL), and the filtrate was reduced in volume to ∼30 mL and cooled to −35 °C. Complex **4** formed as dark-green crystals, which were washed with cold toluene (−78 °C) and dried in vacuo. Yield: 55.5% (0.529 g, 1.08 mmol). Anal. Found (Calcd) for $C_{28}H_{36}Co_2$: C, 68.24 (68.57); H, 7.40 (7.40). ^1H NMR (C_7D_8, 300 MHz): δ 1.93 (s, 24H, CH_3), 1.41 (s, 12H, CH_3). $^{13}C\{^1H\}$ NMR (C_7D_8, 75 MHz): δ 97.8 (s, ring-C), 90.5 (s, ring-C), 53.0 (s, ring-C), 10.7 (s, CH_3), 10.1 (s, CH_3). IR (KBr, cm^{-1}): 2961, 2939, 2894, 2854 (all s, ν_{CH}), 1447 (m, $\nu_{C=C}$), 1376 (s), 1260 (m), 1095 (m), 1028 (s), 805 (m). HRMS (EI): *m/z* calcd for $C_{28}H_{36}Co_2$ (M), 490.1481; found, 490.1472. UV λ_{max} (ε_{max}): 406 (1560), 339 (3160), 276 (7200), 251 (14130).

$Pn^*_2Ni_2$ (5). *cis*-$Pn^*(SnMe_3)_2$ (1.00 g, 1.95 mmol) in THF (20 mL) was added to a suspension of $NiCl_2(DME)$ (0.43 g, 1.95 mmol) in THF (50 mL) at room temperature while stirring. The solution changed to a murky orange color and was allowed to stir for 24 h, by which time it had darkened to a red-brown color. The solution was then filtered through Celite on a frit and the volume reduced to ∼20 mL. Pentane (30 mL) was then added and the solution cooled to −78 °C to produce **5** as dark-orange blocky crystals, which were filtered off and washed with cold pentane (−78 °C) before drying. Yield: 36.9% (0.350 g, 0.72 mmol). Anal. Found

(21) Silvester, D. S.; Aldous, L.; Hardacre, C.; Compton, R. G. *J. Phys. Chem. B* **2007**, *111*, 5000–5007.
(22) Calderazzo, F.; De Benedetto, G. E.; Englert, U.; Ferri, I.; Pampaloni, G.; Wagner, T. *Z. Naturforsch., B: Chem. Sci.* **1996**, *51*, 506–516.
(23) Barlow, S. D.Phil. Thesis, University of Oxford, 1996.
(24) Heyn, B.; Hipler, B.; Kreisel, G.; Schreer, H.; Walther, D. *Anorganische Synthesechemie*; Springer-Verlag: Berlin, 1986.
(25) Kermagoret, A.; Braunstein, P. *Organometallics* **2008**, *27*, 88–99.
(26) *ADF*, version 2006.01; Scientific Computing & Modelling NV: Amsterdam, 2006.
(27) Vosko, S. H.; Wilk, L.; Nusair, M. *Can. J. Phys.* **1980**, *58*, 1200–1211.
(28) Becke, A. D. *Phys. Rev. A* **1988**, *38*, 3098–3100.
(29) Perdew, J. P.; Yue, W. *Phys. Rev. B* **1986**, *33*, 8800.
(30) Cloke, F. G. N.; Green, J. C.; Jardine, C. N.; Kuchta, M. C. *Organometallics* **1999**, *18*, 1087–1090.
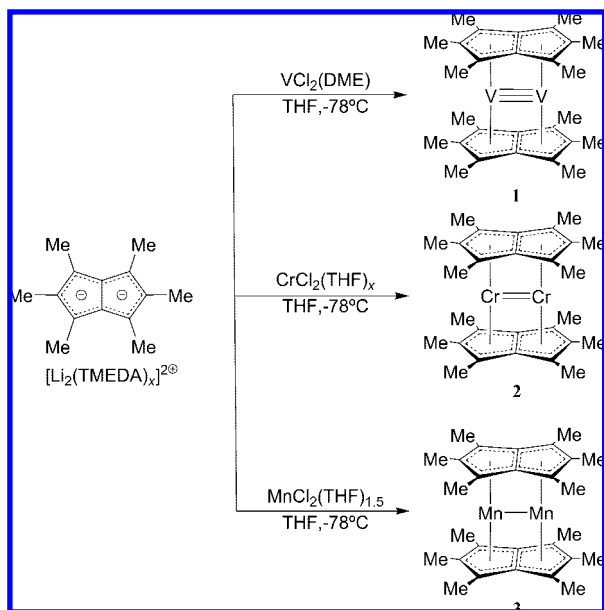
(Calcd) for $C_{28}H_{36}Ni_2$: C, 68.69 (68.64); H, 7.48 (7.41). ^{1}H NMR (C_7D_8, 300 MHz): δ 2.40 (s, 12H, CH_3), 1.43 (s, 24H, CH_3). ^{13}C{^{1}H} NMR (C_7D_8, 75 MHz): δ 93.6 (s, ring-*C*), 90.9 (s, ring-*C*), 68.1 (s, ring-*C*), 11.4 (s, CH_3), 10.1 (s, CH_3). IR (KBr, cm^{-1}): 2957, 2937, 2899, 2853 (all s, ν_{CH}), 1444 (m, $\nu_{C=C}$), 1374 (s), 1262 (m), 1092 (m), 1025 (s), 800 (m). HRMS (EI): *m/z* calcd for $C_{28}H_{36}Ni_2$ (M), 488.1524; found, 488.1517. UV λ_{max} (ε_{max}): 729 (1900), 453 (4140), 402 (4770), 355 (10500), 331 (14160), 278 (14800), 241 (13400), 223 (13830).

Pn^*_2 (6). To a mixture of *cis*-$Pn^*(SnMe_3)_2$ (0.25 g, 0.49 mmol) and $FeCl_2(THF)_{1.5}$ (0.11 g, 0.49 mmol) was added THF (20 mL) at room temperature with stirring. The slurry darkened within 2 h, and gradually a black, insoluble solid formed. After 24 h, the solvent was stripped, and the residue was extracted with hexane and filtered through Celite. The volume of the solution was reduced to 2 mL, and then the solution was chromatographed on silica using pentane as eluent, collecting the bright-orange band. Yield: 69.9% (0.063 g, 0.17 mmol). Anal. Found (Calcd) for $C_{28}H_{36}$: C, 90.20 (90.26); H, 9.80 (9.74). ^{1}H NMR ($CDCl_3$, 300 MHz): δ 2.08 (s, 6H, CH_3), 2.07 (s, 6H, CH_3), 1.95 (s, 6H, CH_3), 1.92 (s, 6H, CH_3), 0.95 (s, 6H, CH_3), 0.94 (s, 6H, CH_3). ^{13}C{^{1}H} NMR ($CDCl_3$, 75 MHz): δ 152.5, 146.7, 145.8, 128.3, 125.6, 116.4 (s, ring-*C*); 67.2, 47.2 (s, ring-*C*); 17.4, 15.3, 14.6, 14.1, 11.8, 11.5 (s, CH_3). IR (KBr, cm^{-1}): 2964, 2909, 2854 (all s, ν_{CH}), 1647 (s, $\nu_{C=C}$), 1558 (w), 1458, 1437, 1387, 1370 (all s), 1323, 1243, 1096, 1069, 1052, 1009 (all w). HRMS (EI): *m/z* calcd for $C_{28}H_{36}$ (M), 372.2817; found, 372.2801.

Results and Discussion

Syntheses. The reaction of $Li_2Pn^*(TMEDA)_x$ with $TiCl_2(THF)_y$ afforded an amorphous, insoluble, paramagnetic black powder that resisted purification attempts, thus hindering full characterization. On the other hand $Pn^*_2V_2$ (**1**), $Pn^*_2Cr_2$ (**2**), and $Pn^*_2Mn_2$ (**3**) were synthesized using salt-elimination reactions between the appropriate metal dichloride precursors and $Li_2Pn^*(TMEDA)_x$ in THF solvent at −78 °C (Scheme 1). In the case of **1**, it was found that use of $VCl_2(DME)$ [formed from the oxidation of bis(mesitylene)vanadium(0) with Ph_3-CCl][22] was crucial in obtaining the target compound. This adduct is thought to have a polynuclear structure with all-bridging chlorides, thus facilitating reaction of the Pn^* synthon with two vanadium centers in a syn-facial manner. Alternative
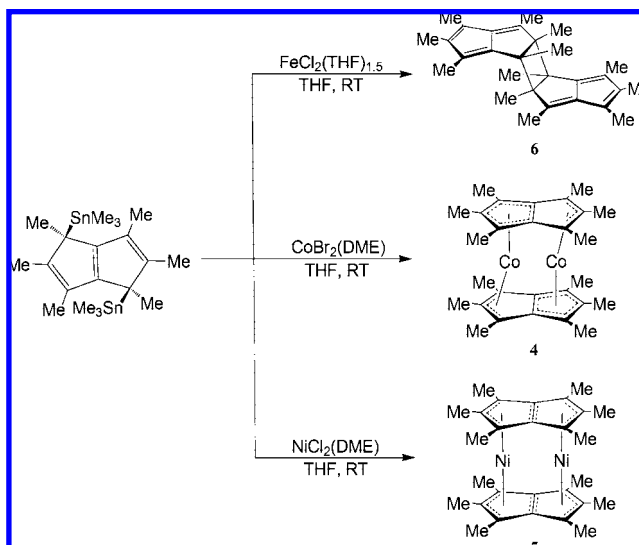
V(II) starting materials such as $VCl_2(pyr)_4$, $VCl_2(TMEDA)_2$,[31] and $V_2Cl_3(THF)_6Zn_2Cl_6$[32] failed to produce **1**, and it is thought that for the former two, this is a consequence of the monomeric nature of the V(II) material, whereas it is possible that reduction of $(V_2Cl_3)^+$ by the permethylpentalene dianion inhibits reaction for the latter. The isolation of **1** was further complicated by an orange-brown impurity that exhibited almost identical solubility properties, and high-vacuum sublimation (125 °C) offered the only means of purification; the elevated temperatures unfortunately led to substantial decomposition, resulting in a very low yield.

The syntheses of **2** and **3** were more straightforward. Activation of anhydrous MCl_2 (M = Cr, Mn) with THF solvent was performed in situ prior to addition of the dilithium salt (Scheme 1). Soxhlet extraction of the residue following removal of THF and subsequent crystallization permitted the facile isolation of crystalline **2** and **3**.

The reaction of $Li_2Pn^*(TMEDA)_x$ with anhydrous M(II) halides in order to prepare $Pn^*_2Co_2$ (**4**) and $Pn^*_2Ni_2$ (**5**) and in the attempted synthesis of $Pn^*_2Fe_2$ gave only intractable solids. We presume that the failure to isolate **4** and **5** was due to uncontrolled oxidation of the powerfully reducing dianion reagent. Consequently, reaction of the softer Pn^* transfer synthon *cis*-$Pn^*(SnMe_3)_2$ with either $CoBr_2 \cdot DME$ or $NiCl_2 \cdot DME$ gave transmetalation to Me_3SnX (X = Br, Cl) and **4** or **5**, respectively (Scheme 2).

Compounds **1**–**5** are sparingly soluble in aliphatic hydrocarbons and only moderately so in aromatic and ethereal solvents; chlorinated solvents serve only to destroy **1**–**3**. While all of the compounds sublime under high vacuum and elevated temperatures (>120 °C), extensive decomposition results, and the sublimate must be washed with pentane to remove a yellow, oily byproduct, which could not be characterized by either ^{1}H NMR spectroscopy or mass spectrometry. Compounds **1**–**3** are unstable to atmospheric moisture and oxygen, instantly decomposing into brown, tarry substances upon exposure; **1** and **3** should be regarded as *extremely* air-sensitive. Solutions of **4**

(31) Edema, J. J. H.; Stauthamer, W.; Van Bolhuis, F.; Gambarotta, S.; Smeets, W. J. J.; Spek, A. L. *Inorg. Chem.* **1990**, *29*, 1302–1306.
(32) Bouma, R. J.; Teuben, J. H.; Beukema, W. R.; Bansemer, R. L.; Huffman, J. C.; Caulton, K. G. *Inorg. Chem.* **1984**, *23*, 2715–2718.

Table 1. Selected Bond Distances and Crystallographic Parameters for **1**−**5**[a]

	1	2	3	4	5
			Bond Distances (Å)		
M−C1	2.2320(16)	2.127(2)	2.1029(17)	2.0576(15)	2.131(2)
M−C2	2.2611(16)	2.154(2)	2.1023(17)	2.0262(15)	2.008(2)
M−C3	2.2337(16)	2.130(2)	2.1109(17)	2.0651(15)	2.116(2)
M−C4	2.2863(16)	2.220(2)	2.2337(16)	2.1392(14)	2.355(2)[b]
M−C5	2.2374(16)	2.125(2)[b]	2.1098(16)	2.0570(14)	2.118(2)[b]
M−C6	2.2552(16)	2.145(2)[b]	2.0912(17)	1.9674(15)	1.998(2)[b]
M−C7	2.2276(16)	2.125(2)[b]	2.1063(17)	2.0529(15)	2.149(2)[b]
M−C8	2.2921(16)	2.223(2)	2.2401(16)	2.1409(14)	2.377(2)[b]
M−C4	2.3017(16)[b]	2.220(2)	2.2541(17)[b]	2.3969(14)[b]	2.335(2)
M−C8	2.2891(16)[b]	2.222(2)[b]	2.2484(16)[b]	2.3878(15)[b]	2.332(2)
avg M−C	2.2720(16)	2.169(2)	2.1703(17)	2.1291(15)	2.192(2)
C1−C2	1.429(2)	1.440(3)	1.441(3)	1.443(2)	1.446(4)
C2−C3	1.430(2)	1.440(3)	1.440(2)	1.446(2)	1.442(4)
C3−C4	1.451(2)	1.455(3)	1.453(2)	1.441(2)	1.433(3)
C4−C5	1.455(2)[b]	1.452(3)	1.453(2)[b]	1.458(2)[b]	1.429(3)
C5−C6	1.427(2)	1.440(3)	1.442(2)	1.443(2)	1.451(3)
C6−C7	1.430(2)	1.444(3)	1.443(2)	1.449(2)	1.440(4)
C7−C8	1.457(2)[b]	1.459(3)	1.456(2)[b]	1.460(2)[b]	1.427(3)
C8−C1	1.452(2)	1.459(3)	1.453(2)	1.439(2)	1.431(3)
C4−C8	1.446(2)	1.454(3)	1.449(2)	1.440(2)	1.472(3)
			Unit-Cell Parameters		
β (deg)	107.9954(10)	108.0132(15)	108.2419(18)	110.3480(10)	108.6695(16)
a (Å)	9.5132(2)	9.6330(2)	9.6431(3)	9.55740(10)	9.6285(3)
b (Å)	12.6438(3)	12.2559(3)	12.3057(3)	12.4752(2)	12.3192(4)
c (Å)	10.2950(3)	10.2796(3)	10.2368(3)	10.1440(2)	10.2589(4)
V (Å^3)	1177.74(5)	1154.14(5)	1153.70(6)	1134.02(3)	1152.83(7)

[a] All of the listed compounds crystallize in the monoclinic space group $P2_1/n$ with Z = 2. [b] One atom in this bond was generated by the inversion symmetry operator.

and **5** decompose within minutes in the presence of air, yet the process takes a few hours in the solid state. All of the compounds gave satisfactory elemental analyses, and each exhibited a molecular ion in its mass spectrum at the accurate mass for the target elemental composition, with subsequent fragmentation suggesting the original molecule to comprise two Pn* units and two metal centers. The IR spectra (4000−700 cm^{-1}) of all five compounds were almost identical, showing bands corresponding to C−H stretches and deformations of the Pn* unit in the ranges 3000−2800 and 1500−1350 cm^{-1}, respectively, as well as two bands in the range 1000−1100 cm^{-1}, all of which could be correlated with the IR data reported for the Cp*$_2$M (M = V−Ni) series[33] and support a planar methylated cyclopentadienyl moiety in both sets of compounds.

In view of the significance of ferrocene (Cp$_2$Fe) in organometallic chemistry and the existence of a wide variety of cyclopentadienyl/indenyl/fluorenyl derivatives,[34] it was extremely surprising not to have isolated any iron-containing complex from the reaction of *cis*-Pn*(SnMe$_3$)$_2$ and FeCl$_2$-(THF)$_{1.5}$. Previous MO calculations have suggested that Pn$_2$Fe$_2$

should exist as an S = 1 bimetallic complex,[35] yet Katz could only obtain the mononuclear ring-bridged (η^5-Pn)$_2$Fe species from the reaction of FeCl$_2$ with Li$_2$Pn in THF, as determined on the basis of ^{1}H NMR spectroscopy, mass spectrometry, and elemental analysis;[11] crystallographic analysis confirmed this assignment a year later.[36] The products from the attempted transmetalation reaction were metallic iron, Me$_3$SnCl, and the [2 + 2] dimer of permethylpentalene, Pn*$_2$ (**6**), indicating that the reaction corresponds to a two-electron oxidation of *cis*-Pn*(SnMe$_3$)$_2$ by Fe(II) and constitutes a viable synthetic route to **6** in good yield. DFT calculations may be able to offer a rationale for this surprising result (see below).

Structural Data. Single crystals suitable for X-ray diffraction were grown by slow cooling to −35 °C of saturated solutions of compounds **1**−**5** in toluene. All of the compounds crystallize in the monoclinic space group $P2_1/n$ and have two formula units in the unit cell. Primary structural and crystallographic parameters are presented in Table 1, while other derived geometrical information is displayed in Table 2. The averages of the intraligand C−C bond lengths for **1**−**5** (in the range 1.44−1.45 Å) imply that the Pn* carbocycle in each case can be considered delocalized and aromatic, with reference to benzene (1.40 Å).[37] The molecular structure of **1** is shown in Figure 1. The average V−C distance is 2.272(2) Å, which is identical to that observed for Cp*$_2$V;[38] the V−Ct (Ct = ring centroid) distance of 1.901(2) Å is also very similar to the values of 1.91 Å and 1.92 Å found

(33) Robbins, J. L.; Edelstein, N.; Spencer, B.; Smart, J. C. *J. Am. Chem. Soc.* **1982**, *104*, 1882−1893.

(34) (a) Plenio, H. *Organometallics* **1992**, *11*, 1856−1859. (b) Bradley, C. A.; Flores-Torres, S.; Lobkovsky, E.; Abruna, H. D.; Chirik, P. J. *Organometallics* **2004**, *23*, 5332−5346. (c) Federman Neto, A.; Pelegrino, A. C.; Darin, V. A. *Trends Organomet. Chem.* **2002**, *4*, 147−169. (d) Murphy, V. J.; O'Hare, D. *Inorg. Chem.* **1994**, *33*, 1833−1841. (e) O'Hare, D.; Green, J. C.; Marder, T.; Collins, S.; Stringer, G.; Kakkar, A. K.; Kaltsoyannis, N.; Kuhn, A.; Lewis, R.; Mehnert, C.; Scott, P.; Kurmoo, M.; Pugh, R. *Organometallics* **1992**, *11*, 48−55. (f) Moss, J.; Thomas, J.; Ashley, A.; Cowley, A. R.; O'Hare, D. *Organometallics* **2006**, *25*, 4279−4285. (g) Curnow, O. J.; Fern, G. M. *J. Organomet. Chem.* **2005**, *690*, 3018−3026. (h) Crisp, J. A.; Meredith, M. B.; Hanusa, T. P.; Wang, G.; Brennessel, W. W.; Yee, G. T. *Inorg. Chem.* **2005**, *44*, 172−174.

(35) Bendjaballah, S.; Kahlal, S.; Costuas, K.; Bevillon, E.; Saillard, J.-Y. *Chem.−Eur. J.* **2006**, *12*, 2048−2065.

(36) Churchill, M. R.; Lin, K. K. G. *Inorg. Chem.* **1973**, *12*, 2274−2279.

(37) Stezowski, J. J.; Hoier, H.; Wilhelm, D.; Clark, T.; Schleyer, P. v. R. *J. Chem. Soc., Chem. Commun.* **1985**, 1263−1264.

(38) Gambarotta, S.; Floriani, C.; Chiesi-Villa, A.; Guastini, C. *Inorg. Chem.* **1984**, *23*, 1739−1747.

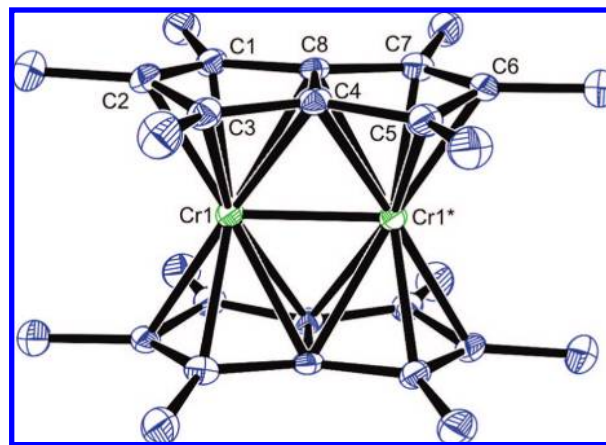***Table 2.*** Summary of Calculated and Experimental Parameters for 1−5[a]

	1	2	3	4	5
S	*0*	*0*	*1*	*0*	*0*
M−M distance	2.169	2.150	2.277	2.491	2.569
	2.12	*2.15*	*2.27*	*2.56*	*2.68*
avg C−C distance	1.442	1.449	1.448	1.447	1.441
	1.45	*1.45*	*1.45*	*1.45*	*1.45*
avg M−C distance	2.262	2.1695	2.160	2.129	2.191
	2.29	*2.19*	*2.17*	*2.15*	*2.25*
M−Ct distance	1.900	1.785	1.774	1.688	1.81
	1.901	*1.788*	*1.778*	*1.798*	*1.83*
Δ	0.0555	0.0842	0.1316	0.0895	0.2770
	0.0463	0.0925	0.1488	0.3672	0.2500
	0.02	*0.06*	*0.11*	*0.06, 0.37*	*0.35*
fold angle	2.89	0.70	1.18	2.04	2.76
	2	*4*	*7*	*5*	*5*
hinge angle	6.97, 7.25	9.30, 9.11	8.21, 7.85	2.80, 11.14	3.25, 3.68
	8	*10*	*7*	*2, 13*	*4*
M−M bond order	*2.83*	*1.98*	*1.13*	*−0.59*	*0.03*

[a] Distances and angles are given in angstroms and degrees, respectively. Calculated values are shown in italics and were determined for ground states with D_{2h} symmetry, except in the case of **4**, where no symmetry was imposed. Calculated bond orders were obtained from the fragment analysis.
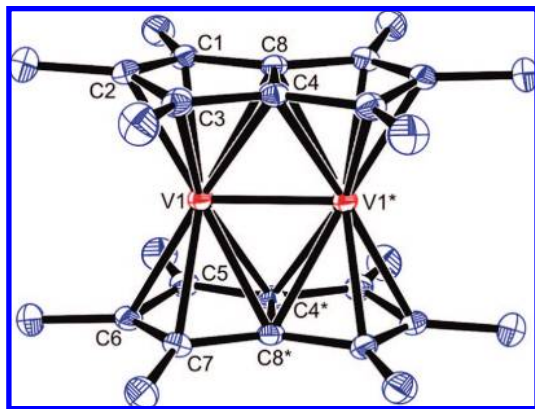
Figure 1. Side view of the molecular structure of **1** with thermal ellipsoids set at 50%. Atoms V1*, C4*, and C8* were generated by inversion symmetry. H atoms have been omitted for clarity.

for Cp*$_2$V and Cp$_2$V, respectively,[39] suggesting similar η^5 bonding environments in each case. The "hinge angle" (ϕ) of a pentalene complex is defined as the angle between the best plane containing the bridgehead atoms (in this example, C4 and C8) and the adjacent wing carbons (C1 and C3) in a C$_5$ ring and the best plane containing the wing carbon atoms (C1 and C3) and the wing-tip atom (C2) (see Figure 6b); essentially, it is a measure of the deviation of the wing-tip atom of the Pn* unit from planarity in the direction away from the metal center.

V metal−metal bonds are rare in comparison to the plethora of examples documented for dichromium complexes.[40] The V−V distance of 2.1689(5) Å is significantly shorter than a V−V single bond [the average distance in the Cambridge Structure Database (CSD) was found to be 2.830 Å] and also than the distance of 2.538 Å found in another vanadium pentalene complex, (CpV)$_2$(μ:η^5,η^5-Pn);[41] V−V triple bonds

(39) Rogers, R. D.; Atwood, J. L.; Foust, D.; Rausch, M. D. *J. Cryst. Mol. Struct.* **1981**, *11*, 183–188.
(40) *Multiple Bonds Between Metal Atoms*, 3rd ed.; Cotton, F. A.; Murillo, C. A.; Walton, R. A., Eds.; Springer: New York, 2005.
(41) Jones, S. C.; O'Hare, D. *Chem. Commun.* **2003**, 2208–2209.

Figure 2. Side view of the molecular structure of **2** with thermal ellipsoids set at 50%. Atom Cr1* was generated by inversion symmetry. H atoms have been omitted for clarity.

have been reported to vary in length from 1.978 to 2.462 Å,[42,43] and it thus appears appropriate to designate the V−V bond in **1** as having a bond order of 3. Although shorter V−V distances have been reported, all of those systems incorporate formamidinate ligands bridging a V$_2$$^{4+}$ core,[44,45] and as such are electronically dissimilar. The shortest existing bond for any divanadium organometallic compound is that reported for (μ: η^5,η^6-Ind)$_2$V$_2$, which has been proposed to contain a triple bond at a distance of 2.351 Å;[46] since both compounds contain only bridging carbocyclic π-based ligands, this is an excellent comparison. It can be seen that **1** contains a substantially shorter internuclear distance; in fact, **1** has the shortest V−V distance of any divanadium organometallic species reported to date. Thus, it can be envisaged that each of the two d^3 V(II) centers has contributed all three of its d electrons toward metal−metal bonding, allowing each metal center to achieve a stable electron count of 18. However, designation of bond order from internuclear distances is less certain in complexes with bridging ligands, where the metals can be forced into close proximity in order to maximize favorable metal−ligand interactions without formally populating metal−metal bonding orbitals.[40,47]

Figure 2 shows the molecular structure of **2**. The average Cr−C distance of 2.169(2) Å and the Cr−Ct distance of 1.785(2) Å are almost identical to the values found in Cp*$_2$Cr and Cp$_2$Cr and suggest almost identical bonding scenarios in each case.[48] The average C−C bond length of 1.449 Å is in very good agreement with the corresponding distance calculated for the nonmethylated double-sandwich analogue Pn$_2$Cr$_2$ (1.446 Å).[35]

There are myriad examples of Cr−Cr multiple bonds in the literature, far more than for other first-row transition metals, and in particular, quadruple bonds between Cr(II) centers have been reported. The large range of internuclear distances for

(42) Cotton, F. A.; Daniels, L. M.; Murillo, C. A. *Angew. Chem., Int. Ed. Engl.* **1992**, *31*, 737–738.
(43) Cotton, F. A.; Frenz, B. A.; Kruczynski, L. *J. Am. Chem. Soc.* **1973**, *95*, 951–952.
(44) Cotton, F. A.; Daniels, L. M.; Murillo, C. A. *Inorg. Chem.* **1993**, *32*, 2881–2885.
(45) Cotton, F. A.; Hillard, E. A.; Murillo, C. A.; Wang, X. *Inorg. Chem.* **2003**, *42*, 6063–6070.
(46) Jonas, K.; Ruesseler, W.; Krueger, C.; Raabe, E. *Angew. Chem.* **1986**, *98*, 905–906.
(47) Poumbga, C.; Daniel, C.; Benard, M. *J. Am. Chem. Soc.* **1991**, *113*, 1090–1102.
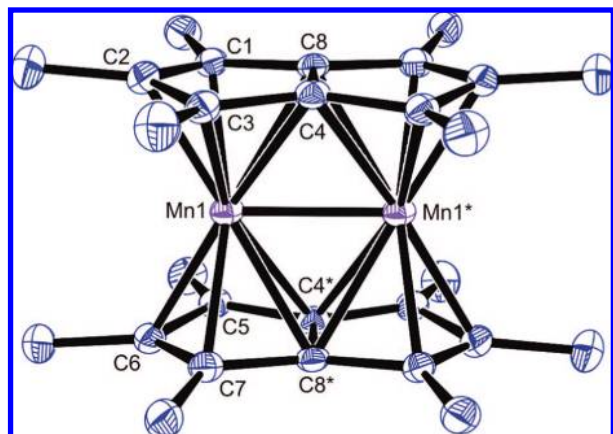(48) Flower, K. R.; Hitchcock, P. B. *J. Organomet. Chem.* **1996**, *507*, 275–277.

Figure 3. Side view of the molecular structure of **3** with thermal ellipsoids set at 50%. Atoms Mn1*, C4*, and C8* were generated by inversion symmetry. H atoms have been omitted for clarity.

Cr−Cr quadruple bonds (1.829−2.531 Å in the CSD) has led to the introduction of the definitions "short" and "supershort" (<1.90 Å).[40] Recently, even shorter bonds between Cr(I) have been established, suggesting that even higher bond orders are possible within the $D_{\infty h}$ core, albeit using a rather empirical treatment.[49−51] The Cr−Cr separation of 2.1494(7) Å in **2** is even shorter than the corresponding distance of 2.251 Å in the closest structural analogue, $(\mu:\eta^5,\eta^5\text{-C}_8\text{H}_4{}^{1,4\text{-iPr}_3\text{Si}})_2\text{Cr}_2$, which has a calculated bond order of 1.67.[15] On the basis of this comparison and electron-counting considerations, it was deemed appropriate to assign a bond order close to 2, since this would give each Cr center in **2** an 18-electron configuration, and the compound would also be expected to be diamagnetic, as is **1**. Since the corresponding distance in **2** would fall into the "short" quadruple bond range as designated by Cotton,[40] it serves as an example of the fact that bond order may be difficult to assign using internuclear distances alone.

The molecular structure of **3** (Figure 3) demonstrates that the two Mn centers are bound almost symmetrically, with both bonding in an η^5 fashion to the Pn* ligands. There is, however, a slight tendency toward $\eta^5:\eta^3$ coordination for the metal centers, as indicated by their ring-slippage (Δ) values of 0.132 and 0.149 Å (see Figure 6 for the definition of Δ). The mean Mn−C distance of 2.170(2) Å is almost identical to the value of 2.169(5) Å found in low-spin Cp*$_2$Mn.[52] No comparison can be drawn from high-spin Cp$_2$Mn since it exists as a nonsandwich polymer in the solid state,[53] although gas-phase electron diffraction has been performed on the molecule and gives a mean M−C distance of 2.380(6) Å.[54] The similarity of **3** to Cp*$_2$Mn implies that the manganese centers are also low-spin. The Mn−Ct distances for the two species are reasonably similar, with values of 1.776 and 1.734 Å for **3** and Cp*$_2$Mn, respectively. The Mn−Mn distance of 2.277(5) Å in **3** is the second-shortest to be documented, the only shorter one being the separation of

2.170 Å for the formal Mn−Mn triple bond in $(\text{CpMn})_2(\mu\text{-CO})_3$[55] [a single Mn−Mn bond has been described at an internuclear distance of 2.7−2.8 Å between two Mn(II) centers].[56] This short internuclear distance suggests that multiple-bond character is present, but as the above discussion has established, bond orders cannot necessarily be determined from interatomic distances when bridging ligands are involved; it should be noted, however, that a single bond would achieve an 18-electron count for each Mn center. The recently synthesized analogue $(\mu:\eta^5,\eta^5\text{-C}_8\text{H}_4{}^{1,4\text{-iPr}_3\text{Si}})_2\text{Mn}_2$ demonstrates a mixed-spin bimetallic nature with two extremes of coordination: one Mn is bound in an $\eta^5:\eta^5$ fashion and the other in an $\eta^1:\eta^1$ fashion, with a localized C−C double bond in the latter C$_5$ ring.[14] The two pentalene rings are not eclipsed but tilt away from one another at angles of 24 and 11°, respectively; this is presumably due to a subtle interplay between the bonding requirements of the two mixed-spin metals and to a sterically induced twist from the large Si^{i}Pr$_3$ groups, as was reported for $(\mu:\eta^5,\eta^5\text{-C}_8\text{H}_4{}^{1,4\text{-iPr}_3\text{Si}})_2\text{Mo}_2$.[16] The Mn−Mn distance of 2.609 Å is considered short enough to constitute a weak single metal−metal bond; DFT calculations on Pn$_2$Mn$_2$ have determined a fractional bond order of 0.6, with the molecule displaying C_{2v} molecular symmetry having one Mn center bound in an $\eta^5:\eta^5$ coordination and the other biased toward an $\eta^3:\eta^3$ arrangement.[35]

The crystal structure of **4** (Figure 4) shows the molecule to be centrosymmetric, with each Pn* fragment bonded in an η^5: η^3 fashion. The Co−Ct distance of 2.69 Å to the η^5-coordinated ring is substantially shorter than that for the η^3 ring, as expected since in one instance the metal is bonding to all of the carbons in the cyclopentadienyl moiety and in the other its main interaction is with the nonbridgehead carbons. The ring slippage varies significantly, from 0.367 Å for the η^3 mode to 0.089 Å for the η^5 mode, demonstrating an overall shearing of the two Pn* ligands relative to one another in a direction perpendicular to the plane that bisects the ring systems. A consequence of this distortion is the bending away of the wing-tip carbon, which must do so in order to maximize overlap with the displaced Co atom. Theoretical calculations have anticipated that there would be no significant metal−metal interaction in the nonmethylated analogue,[35,57] for which Co−Co distances of 2.60 Å have been computed; this is in contradiction to the distance of 2.491(2) Å observed in the crystal structure of **4**, which is indicative of a typical Co−Co single bond (the mean value for compounds listed in the CSD is 2.530 Å). However, as each Co center formally has an electron count of 18 in the observed coordination environment, a direct Co−Co interaction is not necessary to achieve stability.

The molecular structure of **5** (Figure 5) clearly shows that the bonding description in the molecule may be best described as two η^3-allyl interactions, which is reasonable since each Ni would achieve an electron count of 16; this parallels the known stability of $\text{trans-}(\mu:\eta^3,\eta^3\text{-Pn})[\text{Ni}(\eta^3\text{-C}_3\text{H}_5)]_2$.[58] This structure results in a long Ni−Ni separation of 2.569(1) Å. The mean Ni−C distance of 2.192(2) Å for **5** is marginally longer than the 2.146 Å observed for $\text{trans-}(\mu:\eta^3,\eta^3\text{-Pn})[\text{Ni}(\eta^3\text{-C}_3\text{H}_5)]_2$. The ring slippage values are similar for the Ni centers in **5** (0.277 Å and 0.250 Å), and each is larger than the corresponding value

(49) Nguyen, T.; Sutton, A. D.; Brynda, M.; Fettinger, J. C.; Long, G. J.; Power, P. P. *Science* **2005**, *310*, 844–847.

(50) Kreisel, K. A.; Yap, G. P. A.; Theopold, K. H. *Inorg. Chem.* **2008**, *47*, 5293–5303.

(51) Kreisel, K. A.; Yap, G. P. A.; Dmitrenko, O.; Landis, C. R.; Theopold, K. H. *J. Am. Chem. Soc.* **2007**, *129*, 14162–14163.

(52) Freyberg, D. P.; Robbins, J. L.; Raymond, K. N.; Smart, J. C. *J. Am. Chem. Soc.* **1979**, *101*, 892–897.

(53) Elschenbroich, C.; Salzer, A. *Organometallics: A Concise Introduction*, 2nd revised ed.; VCH: Weinheim, Germany, 1992.

(54) Haaland, A. *Inorg. Nucl. Chem. Lett.* **1979**, *15*, 267–269.

(55) Bernal, I.; Korp, J. D.; Herrmann, W. A.; Serrano, R. *Chem. Ber.* **1984**, *117*, 434–444.

(56) Kheradmandan, S.; Fox, T.; Schmalle, H. W.; Venkatesan, K.; Berke, H. *Eur. J. Inorg. Chem.* **2004**, 3544–3554.

(57) Burdett, J. K.; Canadell, E. *Organometallics* **1985**, *4*, 805–815.

(58) Miyake, A.; Kanai, A. *Angew. Chem., Int. Ed. Engl.* **1971**, *10*, 801–802.
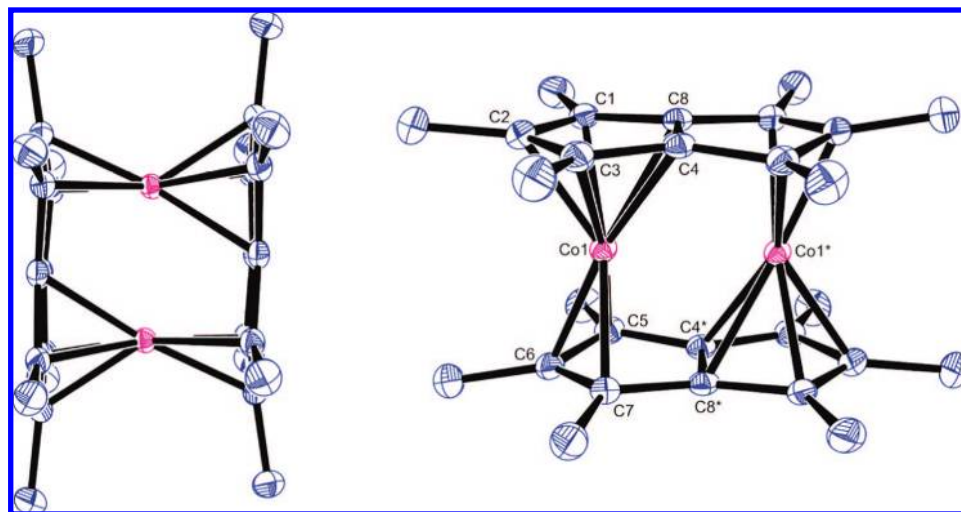
Figure 4. (left) Tilted view and (right) side view of the molecular structure of **4** with thermal ellipsoids set at 50%. Atoms Co1*, C4*, and C8* were generated by inversion symmetry. H atoms have been omitted for clarity.
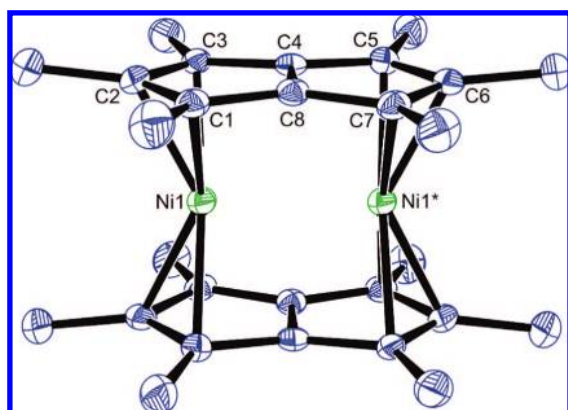

Figure 5. Side view of the molecular structure of **5** with thermal ellipsoids set at 50%. Atom Ni1* was generated by inversion symmetry. H atoms have been omitted for clarity.
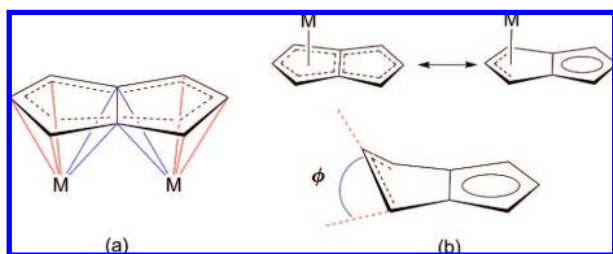

Figure 6. (a) Metal to ring-junction-carbon distances $M-C_J$ (blue lines) and metal to wing-tip-carbon distances $M-C_W$ (red lines) used to calculate the ring slippage, Δ [where $\Delta \equiv \sum(M-C_J)/2 - \sum(M-C_W)/3$]. (b) Schematic illustration showing the definition of the hinge angle (ϕ) used in the structural discussion of the $Pn^*_2M_2$ complexes **1**–**5**.

for *trans*-(η^3,η^3-C_8H_6)[Ni(η^3-C_3H_5)]$_2$ (0.207 Å), demonstrating a greater degree of displacement that can be ascribed to the greater repulsive interaction encountered when the metals are cis-bound in the homoleptic species. The Ni–Ct distances (1.81 Å and 1.83 Å) in **5** are almost identical to that found in nickelocene (1.82 Å).[59] The temptation might arise to describe this compound as two independent bis(allyl)Ni units bridged by two pairs of bridgehead-C atoms, but such a description

(59) Seiler, P.; Dunitz, J. D. *Acta Crystallogr.* **1980**, *B36*, 2255–2260.

Table 3. Summary of the Solution ^1H and ^{13}C NMR Chemical Shift Data (ppm) for **1**–**5** in C_7D_8[a]

compound	^1H		$^{13}C\{^1H\}$			
	WT-CH$_3$	W-CH$_3$	CH$_3$	WT	W	B
$Pn^*_2V_2$	0.87	2.10	12.2	74.1	97.4	86.5
$Pn^*_2Cr_2$[b]	8.97	2.04	–	–	–	–
$Pn^*_2Mn_2$[b]	59.76	−19.15	–	–	–	–
$Pn^*_2Co_2$	1.41	1.93	10.1,10.7	90.5	53.0	97.8
$Pn^*_2Ni_2$	2.40	1.43	10.1,11.4	93.6	68.1	90.9

[a] Notation: WT = quaternary wing-tip carbon atoms; W = quaternary wing carbon atoms; B = bridgehead carbon atoms. [b] No observable resonances in ^{13}C NMR spectrum.

camouflages the fact that the two "allyl" units are intimately linked electronically.[60] This is supported by the C4–C8 bond length of 1.472(3) Å, which does not correspond to that of an isolated C=C bond (1.34 Å).

NMR Spectroscopy. All of the complexes, whether diamagnetic or paramagnetic, exhibit a characteristic solution ^1H NMR spectrum consisting of two singlets in a ratio of 2:1 for wing and wing-tip methyl environments, respectively, indicating that in the solution phase they all exhibit D_{2h} molecular symmetry (Table 3). The solution ^{13}C NMR spectra of **1**, **4**, and **5** show five resonances in the chemical shift regions expected for π-bound pentalene ligands, each having a negligible temperature dependence of its chemical shift, as expected for a diamagnetic complex. No resonances could be observed in the ^{13}C spectra of **2** or **3**. The ^1H NMR data for the unsubstituted analogues Pn_2M_2 (M = Co, Ni) have also been reported and are similarly diamagnetic. This is in direct contrast to the NMR data for the metallocenes Cp_2M and Cp^*_2M (M = V, Mn, Co, Ni), which display significantly shifted and broadened ^1H and ^{13}C resonances as a consequence of their paramagnetism.[1a,53]

The "double chromocene" complex **2** demonstrates a rather different room-temperature ^1H NMR spectrum, with the wing-tip Me resonance being a well-defined singlet at $\delta \approx 2$ ppm (similar to the location found for **1**, **4**, and **5**) and the wing Me shifted to $\delta \approx 9$ ppm with distinct broadening, demonstrative of paramagnetic effects within the molecule. It should be noted that in contrast to **2**, the only other known chromium pentalene

(60) Elschenbroich, C.; Heck, J.; Massa, W.; Nun, E.; Schmidt, R. *J. Am. Chem. Soc.* **1983**, *105*, 2905–2907.

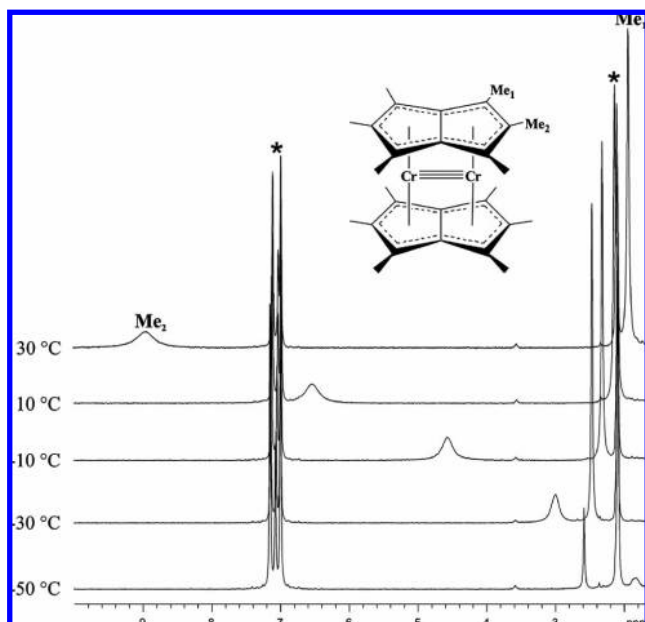**Figure 7.** Variable-temperature ^{1}H NMR spectra of **2** in C$_7$D$_8$ solution.

Figure 8. Temperature variation of the ^{1}H NMR chemical shift for the resonance of the wing-tip methyl group (Me$_2$ in Figure 7) in **2**. Black squares represent experimental data, and the solid line is the least-squares best fit to eq 1.

complex, $(\mu{:}\eta^5{,}\eta^5\text{-C}_8\text{H}_4^{1,4\text{-iPr}_3\text{Si}})_2\text{Cr}_2$, is too paramagnetic to be characterized using NMR methods.[15] The former resonance varies slightly with temperature ($\Delta\delta \approx 1.5$ ppm downfield between 373 and 183 K), while the latter has a much more dramatic response in the opposite direction ($\Delta\delta = 18.5$ ppm upfield over the same temperature range); for neither resonance does the temperature dependence of the chemical shift obey the Curie law ($\delta \propto T^{-1}$). The overall visual effect in the spectrum is that the high-field wing-tip Me resonance is "eclipsed" by the more responsive wing Me peak (Figure 7).

These results are indicative that an $S = 0 \rightleftarrows S = 1$ thermal equilibrium is in operation ($K_{eq} = [\mathbf{2}^*]/[\mathbf{2}]$, where $\mathbf{2}^*$ is the $S = 1$ excited state). Indeed, compounds such as $(\text{CpV})_2(\mu{:}\eta^5{,}\eta^5\text{-Pn})^{41}$ and $(\text{CpV})_2(\mu{:}\eta^5{,}\eta^5\text{-COT})$ (with which **2** is isoelectronic)[60,61] have an $S = 0$ ground state and an $S = 1$ excited state and display similar behavior in their variable-temperature ^{1}H NMR spectra. Thus, we can describe the ground state of **2** as having spin pairing between the Cr centers, giving a diamagnetic $S = 0$ configuration, but these antiferromagnetically coupled electrons can uncouple as the temperature increases, which is equivalent to promoting an electron into a higher electronic state. Conversely, previous DFT calculations have predicted that in Pn$_2$Cr$_2$, the HOMO−LUMO gap is only 0.18 eV, with the excited state being a *singlet*.[35]

This observed process can be described by an equilibrium between the $S = 0$ and $S = 1$ states that can be modeled as a Boltzmann distribution, with the observed chemical shift of the nucleus given by the sum of contributions from diamagnetic and paramagnetic terms (eq 1):[62]

$$\delta_{obs} = \delta_{LS} + \frac{C}{T[1 + e^{(\Delta H\circ - T\Delta S\circ)/RT}]} \quad (1)$$

where δ_{LS} is the limiting (i.e., $T = 0$) chemical shift value for the diamagnetic low-spin (LS) form of the species, C is a

constant related to the isotropic hyperfine coupling constant and magnetic susceptibility of the nucleus of interest, and $\Delta H\circ$ and $\Delta S\circ$ are the thermodynamic values related to $\Delta G\circ$ for the equilibrium reaction. As can be seen in Figure 8, an excellent fit to the experimental data was achieved with $C = 42238$, $\Delta H\circ = 14.9$ kJ mol^{-1}, and $\Delta S\circ = 26.5$ J K^{-1} mol^{-1}; it can thus be calculated that there is a 5.8% population of the triplet state at 300 K.

The endothermicity for the interconversion reflects the greater population of antibonding orbitals by the electrons in the excited state and confirms that the singlet is the ground state, in contrast to the results of theoretical calculations on the unmethylated compound; the larger value found for $\Delta H\circ$ in $(\text{CpV})_2(\mu{:}\eta^5{,}\eta^5\text{-Pn})$ (17.2 kJ mol^{-1}) potentially reflects breaking of a stronger δ bond as opposed to the antibonding δ^* interaction present in **2**. The change in entropy is somewhat larger than that expected on the basis of only the increase in electronic degeneracy within the triplet molecule ($\Delta S\circ = R \ln[(2S_{HS} + 1)/(2S_{LS} + 1)] = 9.13$ J K^{-1} mol^{-1}) and can be ascribed to an increase in the number of accessible rotational and vibrational degrees of freedom in the high-spin (HS) form; values reported for $(\text{CpV})_2(\mu{:}\eta^5{,}\eta^5\text{-Pn})$ and $(\text{CpV})_2(\text{COT})$ are in a similar range. A change in the conformation of the molecule with temperature could also result in alteration of the spin state of **2**, yet almost identical thermodynamic parameters ($\Delta H\circ = 15.0$ kJ mol^{-1}, $\Delta S\circ = 23.3$ J K^{-1} mol^{-1}) are found when the solvent is THF-d_8, whose polarity ($\varepsilon_{\text{THF-}d_8} = 7.6$ at 298 K, compared with $\varepsilon_{\text{toluene-}d_8} = 2.5$) would be expected to favor solvation of one conformational isomer over another. Furthermore, rapid exchange by a donor THF molecule coordinated at Cr may also be discounted, paralleling the observations made by Cloke for the isoelectronic complex $(\mu{:}\eta^5{,}\eta^5\text{-C}_8\text{H}_4^{1,4\text{-iPr}_3\text{Si}})_2\text{Mo}_2$, which shows no propensity to coordinate Lewis bases.

Manganocene and its various alkylated/silylated derivatives have attracted much interest because of the influence of cyclopentadienyl substitution on the spin-crossover behavior of the molecules due to variation of the ligand field and steric requirements.[63] Cloke and co-workers[15] have recently documented an asymmetric manganese pentalene complex, $(\mu{:}\eta^5{,}\eta^1\text{-C}_8\text{H}_4^{1,4\text{-iPr}_3\text{Si}})_2\text{Mn}_2$ that shows complex magnetic properties originating from a thermal equilibrium between an $S = 3$ ground state and an $S = 2$ excited state; again, it has been reported that this pentalene complex is too paramagnetic to be characterized by NMR methods, analogous to its Cr counterpart. Compound **3** displays two resonances in its room temperature

(61) Bachmann, B.; Hahn, F.; Heck, J.; Wuensch, M. *Organometallics* **1989**, *8*, 2523–2543.
(62) (a) Smith, M. E.; Andersen, R. A. *J. Am. Chem. Soc.* **1996**, *118*, 11119–11128. (b) Olson, W. L.; Stacy, A. M.; Dahl, L. F. *J. Am. Chem. Soc.* **1986**, *108*, 7646–7656.
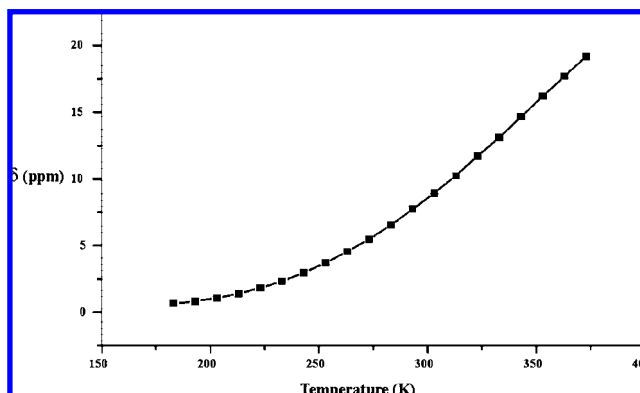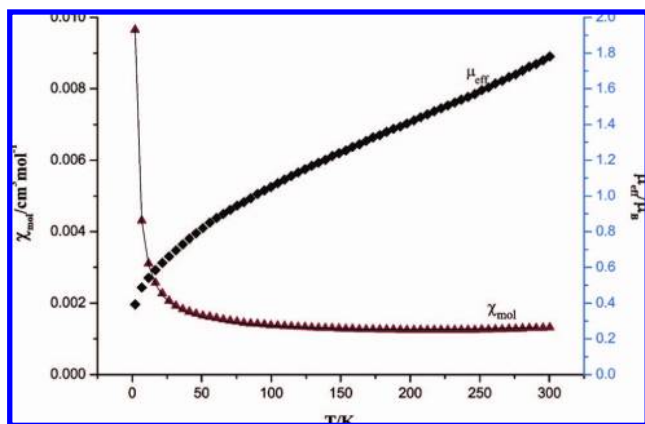
Figure 9. Plots of χ_{mol} (▲, left axis) and μ_{eff} (◆, right axis) vs T for **2** in the solid state. The solid line through the χ_{mol} data represents the least-squares best fit to eq 2.

^{1}H NMR spectrum with the same intensity ratio as the corresponding peaks for **1**, **2**, **4**, and **5**, but these signals are substantially broadened and occur at significantly different chemical shifts compared with those of the other diamagnetic Pn* bimetallic complexes (Table 3). The measured $\Delta\delta$ is significantly larger for the wing Me environments over the temperature range 173–373 K than for the wing-tip methyl protons, which is the opposite behavior found for **2**. In this instance, however, the temperature dependence of each ^{1}H resonance obeys the Curie law, so **3** is best described as a simple Curie paramagnet in solution.

Magnetic Susceptibility Measurements. The solution magnetic moments for **2** and **3** were measured using the Evans method in C_7D_8.[64] At 313 K, the dichromium complex **2** gave an observed solution-phase magnetic moment of $0.57\mu_B$, which is appreciably lower than that predicted from the spin-only formula for a diradical ($\mu_{SO} = g_e[S(S + 1)]^{1/2} = 2.83\mu_B$ using $g_e = 2.0023$ and $S = 1$). If the aforementioned spin equilibrium is assumed, the mole fraction of the triplet state (X_T) may be calculated from $X_T = \mu_{obs}^2/\mu_T^2$, where μ_T is the effective magnetic moment for the triplet state calculated using the spin-only formula.[65] This equation gives an X_T value of 0.072, which compares very well with that predicted using the ^{1}H NMR isotropic-shift method ($K_{313} = 0.079$, $X_T = 0.0732$).

In the solid state, the molar magnetic susceptibility (χ_{mol}) for **2** also did not obey the Curie law. The magnetic moment increases with increasing temperature and agrees with the expected greater population of the paramagnetic excited state. The temperature dependence of χ_{mol} for **2** between 2 and 300 K is shown in Figure 9.

The χ_{mol}-versus-T data are consistent with a spin equilibrium between an $S = 0$ ground state and an $S = 1$ excited state. Such a situation can be modeled using a Bleaney–Bowers expression based on the spin Hamiltonian $\hat{H} = -2J\hat{S}_1\cdot\hat{S}_2$, where $\hat{S}_n$ is the spin-vector operator for the nth atom and J is the

exchange constant between the spins, which is negative for antiferromagnetic coupling, with the triplet state separated in energy from the ground state by $2J$.[66] However, since μ_{eff} does not decrease to zero, the equation is modified to include a term that takes into account a paramagnetic Curie–Weiss-like impurity [likely to be a Cr(III) $S = {}^3/_2$ species arising from oxidation during sample manipulation], and another factor is included to take into account temperature-independent paramagnetism (TIP); these modifications give eq 2:

$$\chi_{mol} = x\left(\frac{5N_Ag_1^2\mu_B^2}{4k(T-\theta)}\right) + (1-x)\left(\frac{2N_Ag_2^2\mu_B^2}{3kT}\right) \times \left(\frac{1}{1+(1/3)e^{(-2J/kT)}}\right) + \text{TIP} \quad (2)$$

where x is the mole fraction of the paramagnetic Curie–Weiss-like impurity and θ is the Weiss constant. Similar expressions have been used to fit the magnetic susceptibilities of other dimer systems. An excellent fit was obtained by least-squares analysis, giving $x = 0.0137$, $J = 462$ cm^{-1}, $\theta = -1.0$ K, and TIP = 1.12×10^{-3} cm^3 mol^{-1}. Cloke has provided a detailed account of Cr–Cr multiple bonding for related compounds in the discussion of $(\mu:\eta^5,\eta^5-C_8H_4^{1,4-iPr_3Si})_2Cr_2$, within which a correlation between the intermetallic distance and the room-temperature magnetic moment has been found for a range of paramagnetic bimetallic dimers of chromium.[15] Complex **2** displays the shortest Cr–Cr distance of this series, which is in support of this conclusion ($\mu_{eff} = 1.76\mu_B$ at 298 K); J for **2** is also one of the highest values reported, as anticipated for a through-space antiferromagnetic coupling model as opposed to a superexchange interaction.

Complex **3** was found to behave as a Curie-like paramagnet in solution (χ_{mol} is proportional to T^{-1}), and the observed effective magnetic moment (μ_{eff}) of $2.79\mu_B$ is very close to the spin-only moment for a triplet molecule ($\mu_{SO} = 2.83$, as shown above). The solid-state magnetic susceptibility data are also in excellent agreement with the solution-phase data, as fits to the Curie–Weiss law gave $\mu_{eff} = 2.78\mu_B$, $C = 0.967$, and $\theta = -1.0$ K.

Electron Spin Resonance. The X-band solution EPR spectrum of **2** was recorded at room temperature and in frozen toluene at 90 K (Figure 10). The room-temperature EPR signal is a very weak isotropic signal at $g = 1.980$. When the sample is cooled to 90 K, the EPR spectrum increases in intensity and changes significantly. At 90 K, a complex signal centered at $g = 1.99$ is now observed, in addition to a broad, weak resonance at $g = 3.999$. This latter feature is centered at 170 mT, which is half the magnetic field of the main signal at 340 mT, and consequently, we have assigned it to the forbidden $\Delta m_S = 2$ transition associated with the small population of $S = 1$ species expected at this temperature.

The room-temperature EPR spectrum of **3** exhibits a broad isotropic signal at $g = 2.005$ (Figure 11) and is consistent with the solution-phase magnetic moment of $2.79\mu_B$ found for **3**. When the sample is cooled to 7.4 K, the spectrum increases in intensity and changes dramatically. This spectrum contains a complex series of overlapping multiplets that to date we have been unable to analyze in detail. It is presumed that the multiplet structure observed at low temperature arises from a complex convolution of g anisotropy, partially resolved Mn hyperfine coupling, and zero-field splitting of the triplet radical **3**.

(63) (a) Robbins, J. L.; Edelstein, N. M.; Cooper, S. R.; Smart, J. C. *J. Am. Chem. Soc.* **1979**, *101*, 3853–3857. (b) Hebendanz, N.; Koehler, F. H.; Mueller, G.; Riede, J. *J. Am. Chem. Soc.* **1986**, *108*, 3281–3289. (c) Switzer, M. E.; Wang, R.; Rettig, M. F.; Maki, A. H. *J. Am. Chem. Soc.* **1974**, *96*, 7669–7674. (d) Ammeter, J. H.; Bucher, R.; Oswald, N. *J. Am. Chem. Soc.* **1974**, *96*, 7833–7834. (e) Koehler, F. H.; Schlesinger, B. *Inorg. Chem.* **1992**, *31*, 2853–2859. (f) Sitzmann, H.; Schar, M.; Dormann, E.; Kelemen, M. *Z. Anorg. Allg. Chem.* **1997**, *623*, 1609–1613.
(64) Schubert, E. M. *J. Chem. Educ.* **1992**, *69*, 62.
(65) Crawford, T. H.; Swanson, J. *J. Chem. Educ.* **1971**, *48*, 382–386.
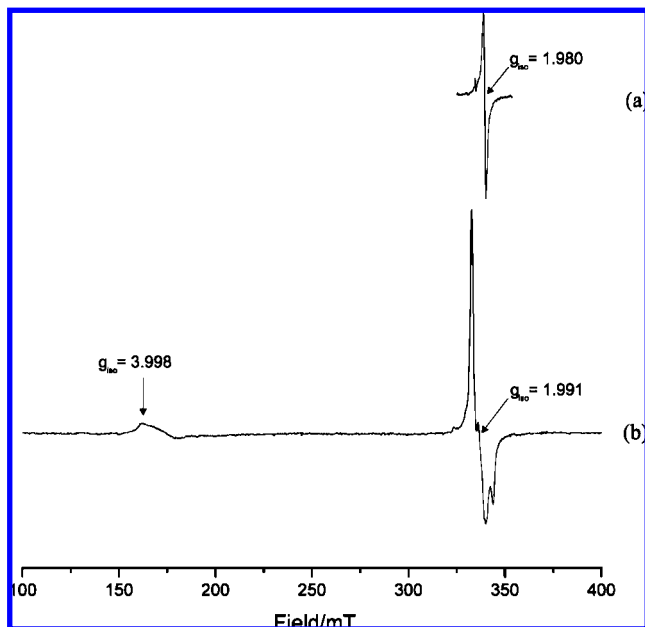(66) Carlin, R. L. *Magnetochemistry*; Springer-Verlag: Weinheim, Germany, 1986.

Figure 10. X-band EPR spectrum for compound **2** in toluene at (a) 298 and (b) 90 K.
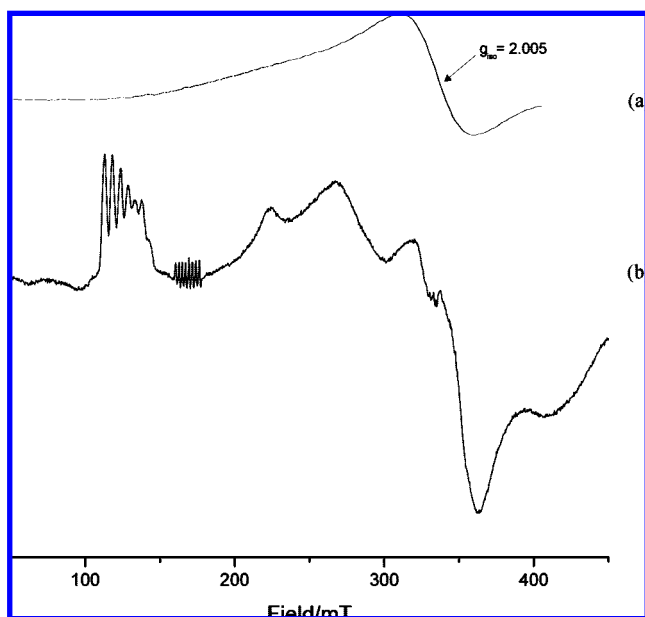

Figure 11. X-band EPR spectrum for compound **3** in toluene at (a) 298 and (b) 7.4 K.

DFT Calculations. Geometry optimizations of Pn*$_2$M$_2$ (M = V−Ni) unequivocally predict a singlet ground state for **1**, **4**, and **5**, as is found experimentally. The calculations for **2** predict a triplet state lying 0.22 eV higher in energy than the singlet ground state, in agreement with what is observed experimentally. A similar ordering was found experimentally for (μ:η^5,η^5-C$_8$H$_4^{1,4\text{-iPr}_3\text{Si}}$)$_2Cr_2$.[15] In this case, both DFT and CASPT2 calculations placed the triplet slightly below the singlet, though the magnetic data suggested the reverse. In all cases, the energy differences are found to be within the accuracy of the calculations. For **3**, a triplet ground state with a singlet lying 0.44 eV higher in energy is predicted, in agreement with experiment.

Geometry optimizations for **1**, **2**, **3**, and **5** resulted in effective D_{2h} symmetry, and consequently, this was imposed for subse-
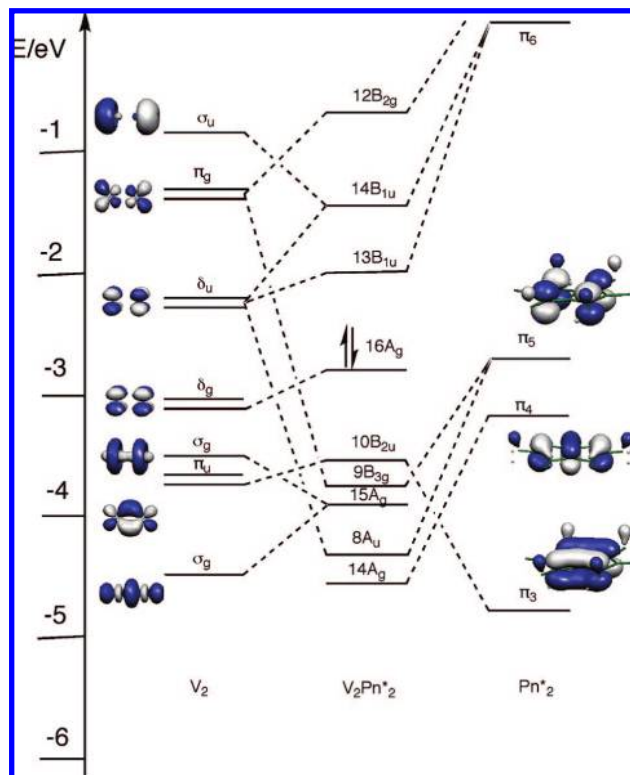

Figure 12. MO scheme for **1** calculated in D_{2h} symmetry, showing the principal levels involved in V−V bonding.

quent frequency calculations and orbital analysis. Conversely, it was discovered that for compound **4**, the lowest-energy structure had effective C_{2h} symmetry, lying 0.57 eV below that of the D_{2h}-optimized structure; similar computational results have been reported for the unsubstituted analogue.[35] Selected geometric parameters are given in Table 2, where they are compared with the experimental values; the agreement with experiment is excellent, with all of the observed trends being reproduced by the calculations.

The synthesis of compounds **1**−**5** has afforded an opportunity to evaluate how the bonding and properties of these compounds evolves across a transition-metal series. MO schemes for bis-(pentalene) metal dimers have been presented previously[16] and are generally in agreement with the one shown in Figure 12 for Pn*$_2$V$_2$. Figure 13 shows the filling of further orbitals as the period is traversed.

Compound **1** is calculated to have the structure with the least ring slippage (Table 2), with both metal atoms experiencing full η^5 coordination. The V−V bond order is calculated as 2.83, with the strongest V−V interactions being embodied in the orbitals 15A$_g$, 10B$_{2u}$, and 16A$_g$ (Figure 12). Thus, to a first approximation, Pn*$_2$V$_2$ can be regarded as having a V−V triple bond with σ, π, and δ components. The consequent short M−M distance appears fully compatible with maximization of bonding to both rings of a permethylpentalene ligand.

It is worth noting at this point that simple electron counting of metal dimers, where the metal−metal bond order, *n*, is predicted from the total electron count, *T*, by the relationship, $36 - T = 2n$, fails in this case, as a quintuple bond would be expected. It is well-established in the case of bridging hydrides, for example, that this simple rule breaks down. A bridging hydride is most consistently treated as donating two electrons to each metal atom. In an analogous manner, one can regard
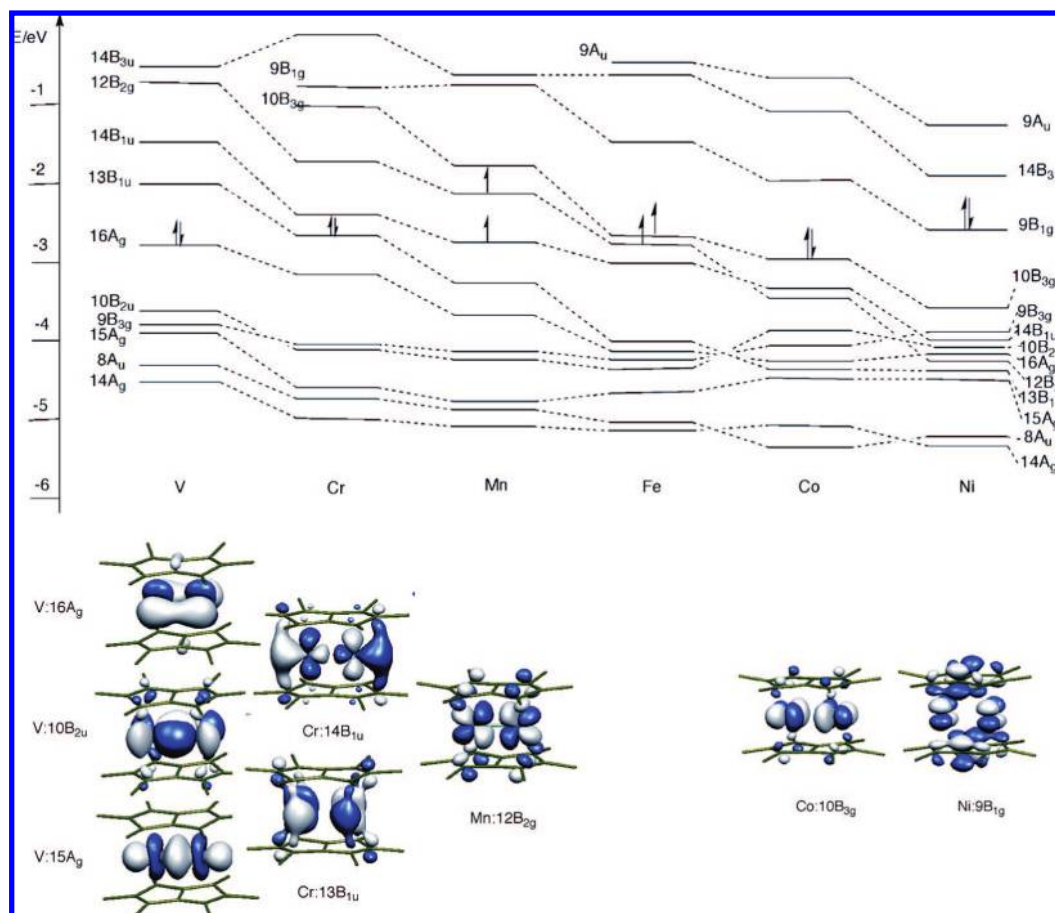
Figure 13. MO scheme for Pn*$_2$M$_2$ (M = V−Ni) complexes (and pertinent MO isosurfaces for isolated compounds) in D_{2h} symmetry, displaying energy-level variations across the series.

the η^5,η^5-pentalene dianion as donating six (or, in a neutral counting scheme, five) electrons to each metal atom. Both of the metal atoms are within bonding distance of the bridgehead carbons and share the two electrons offered by these atoms. Under this counting scheme, with the proposal of a triple bond between the metal atoms, both satisfy the 18-electron count.

For **2** in the $S = 0$ ground state, both electrons are added to the 13B$_{1u}$ orbital, which is Cr−Cr-antibonding (Figure 13). In the $S = 1$ state, this orbital is singly occupied, and the second unpaired electron occupies the 14B$_{1u}$ orbital. These two orbitals are mixtures of δ^* and σ^* orbitals, and consequently, the M−M bond order decreases; the chromium dimer can regarded as having a Cr−Cr double bond (the calculated bond order is 1.98). Because of the similar nature of these two orbitals, the spin state has little effect on the structural parameters.

For **3**, the 13B$_{1u}$ orbital is doubly occupied, and the two unpaired electrons reside in the 14B$_{1u}$ and 12B$_{2g}$ orbitals. The latter is predominantly Mn−Mn π^* in character, so the bond order again decreases; thus, the manganese compound has a Mn−Mn single bond. There is a subsequent lengthening of the M−M distance compared with that in the Cr analogue as well as an increase in the ring slippage.

Topographical analysis of the singly occupied MOs (SOMOs) of **2** and **3** permits an interpretation of the unusual paramagnetic shifts observed in their respective ^{1}H NMR spectra. For **2**, it was found that wing-tip CH$_3$ protons experience the greatest chemical shift range in variable-temperature NMR. The calculated HOMO−LUMO gap is small and supports the finding that the molecule has a low-lying paramagnetic ($S = 1$) state. This

corresponds to occupation of each level by an unpaired electron; examination of the 13B$_{1u}$ and 14B$_{1u}$ MOs (Figure 13) reveals that the wing-tip carbons have large orbital coefficients while the wing carbon atoms make negligible contributions. The former have a correspondingly higher unpaired-spin density, and the protons on the adjacent methyl groups thus experience a greater effect through the paramagnetic contact shift term (σ_p); the latter environment results in a chemical shift much closer to that expected for a diamagnetic molecule.

Conversely, the HOMO and LUMO of **3** (which was experimentally and theoretically found to have an $S = 1$ ground state and thus to have an unpaired electron in each of these orbitals) show some spin density at the wing-tip carbons in 14B$_{1u}$, but the orbital coefficients are now greater at the wing carbon atoms in 12B$_{2g}$ (Figure 13). The resonances in the ^{1}H NMR spectrum of **3** were both found to be broad (because each CH$_3$ group experiences some unpaired-spin density), yet it is the wing CH$_3$ protons that show the greatest perturbation with temperature; this may be explained by the larger coefficients of these positions present in the highest occupied SOMO. A spin-polarization mechanism explains the opposite isotropic shifts to upfield and downfield values for the proton resonances of wing and wing-tip Me groups, respectively, in compounds **2** and **3** and is reminiscent of the effects seen upon replacing a cyclopentadienyl ring proton with that of a methyl group in the series Co$_3$(η^5-Cp^R)$_3$(μ^3-X)$_2$ (Cp^R = C$_5$H$_5$, C$_5$H$_4$Me, X = S; Cp^R = C$_5$Me$_5$, X = CO).[67]

Figure 13 shows the orbital levels for **4** with D_{2h} symmetry. The doubly occupied HOMO is the 10B$_{3g}$ orbital, the antibond-
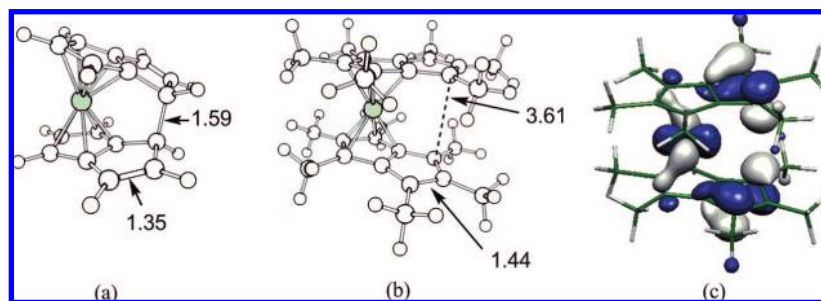
Figure 14. Optimized geometries for (a) Pn_2Fe and (b) Pn^*_2Fe (distances are in Å); (c) HOMO of Pn^*_2Fe.

ing π^* counterpart of the $10B_{2u}$ orbital. However, by this stage the orbitals are becoming more radially contracted, as evidenced by the drop in energy of the $10B_{3g}$ orbital across the period, so the expectation of significant metal−metal interaction is reduced; this factor results in a lowering of the molecular symmetry.

Finally, for **5**, the $9B_{1g}$ orbital becomes fully occupied. Its metal component is a Ni−Ni δ-bonding orbital, but this has a significant out-of-phase interaction with the π orbitals of the bridgehead carbons, which accounts for the large ring slippage and the drive to an $\eta^3:\eta^3$ coordination.

The difficulty experienced in synthesizing $Pn^*_2Fe_2$ has been investigated. A crossover of energy levels results when M = Fe, and it was found that the $S = 1$ species is more stable than the $S = 0$ complex when optimization was conducted under the constraint of D_{2h} symmetry. Relaxation of this parameter revealed that a $Pn^*_2Fe_2$ structure in C_{2v} symmetry ($S = 1$) was found to be the most stable, yet it is notable that when the synthesis of Pn_2Fe_2 was attempted by Katz et al.,[11] only monometallic $(\eta^5\text{-}Pn)_2Fe$ was isolated. In order to investigate the fate of such a species when pentalene is permethylated, geometries were optimized for Pn_2Fe and Pn^*_2Fe. In the former case, an ansa structure was found to be the most stable. In this structure, the two pentalene rings are linked by a C−C bond of 1.59 Å (Figure 14a), and C=C double bonds having lengths of 1.35 Å were located in the uncoordinated five-membered rings; this structure corresponds to the product found experimentally and finally characterized by X-ray crystallography some years later.[36] In the case of the analogous Pn^*_2Fe complex, the two Pn* ligands remain almost parallel to one another, with the methyl groups preventing a sufficiently close approach for C−C bond formation (Figure 14b). The π-electron density on the uncoordinated ring was delocalized, as indicated by C−C bond lengths of 1.44 Å, and the HOMO was largely localized on the uncoordinated rings, showing in-phase lobes between the two nearest carbons, which were 3.61 Å apart (Figure 14c). Thus, despite the fact that this complex is also set up for a C−C link between the Pn* ring systems, steric interaction prevents this, and the rings are aligned parallel to one another so as to maximize bonding to the Fe center. This eventuality would form an unstable open-shell monometallic diradical, which would potentially be predisposed to loss of an Fe atom accompanied by coupling of the rings, since the restriction of Fe−Pn* bonding would be removed. The resultant bis(vinylcyclopentadienyl) diradical would then couple to form the Pn* dimer, which is
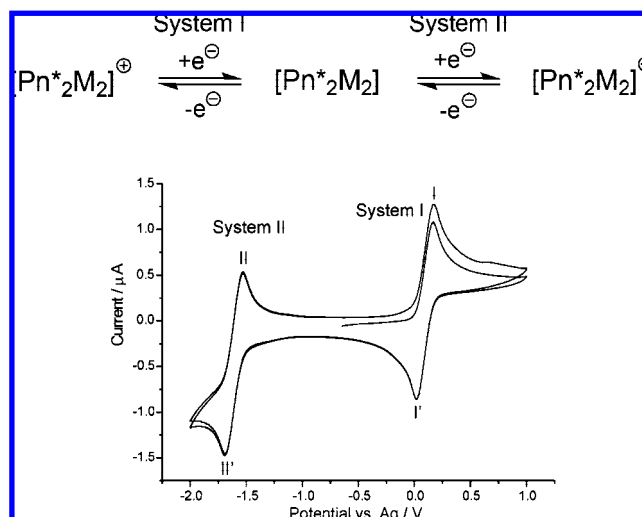
the reverse of the known process found to occur during the photolysis of Pn_2.[68]

Electrochemistry. Cyclic voltammetry experiments were performed on **1**−**5** in dry THF containing 0.1 M [$^nBu_4N$][BF_4] between the potential limits of −2.00 to +1.60 V versus Ag. The general behavior of these complexes is illustrated using the voltammetric response of compound **5** (Figure 15).

For **5**, two redox processes (labeled as systems I and II) are observed, with corresponding oxidation (I and II) and reduction (I′ and II′) peaks in a ratio of 1:1 centered at midpeak potentials of +0.09 and −1.61 V and having peak-to-peak separations, ΔE_p, of 146 and 152 mV, respectively, at a scan rate of 100 mV s^{-1}. It should be noted that these electrochemical events do not display the ideal ΔE_p of 59 mV for a fully reversible single-electron transfer at 298 K, indicating that both systems I and II are quasi-reversible on the voltammetric time scale of the experiment.[69] Similar qualitative behavior was observed for the entire series of studied complexes **1**−**5**, with the midpeak potentials shifted depending on the nature of the metal ions. The measured voltammetric parameters are summarized in Table 4.

For each of the [$Pn^*_2M_2$] complexes, 20 cycles were performed over the potential range encompassing system I and 20 cycles over the potential range encompassing system II (the behavior of **1** is discussed separately below and is not included

Figure 15. Cyclic voltammogram of 1.0 mM **4** in THF containing 0.1 M [$^nBu_4N$][BF_4]. The scan rate was 100 mV s^{-1}.

(67) Horrocks, W. D., Jr. In *NMR of Paramagnetic Molecules: Principles and Applications*; La Mar, G. N.; Horrocks, W. D., Jr.; Holm, R. H., Eds.; Academic: New York, 1973; pp 127−177.

(68) Bally, T.; Zhu, Z.; Neuenschwander, M.; Chai, S. *J. Am. Chem. Soc.* **1997**, *119*, 1869−1875.
(69) Banks, C. E.; Compton, R. G. *Understanding Voltammetry*; World Scientific: Singapore, 2007.

Table 4. Summary of Electrochemical Data for Compounds **1**−**5** and Selected Metallocenes versus the Cp_2Fe^+/Cp_2Fe Couple[a]

compound	$E°$ (V) [complex]$^{+/0}$	[complex]$^{0/-}$	refs
$[Pn^*_2V_2]$	-0.18^b	-2.57	f
Cp_2V	-1.11^c	-3.30^c	73
$[Pn^*_2Cr_2]$	-0.60	-1.95	f
Cp^*_2Cr	-1.44^d		33
Cp_2Cr	-1.07^d	-2.68^d	73
$[Pn^*_2Mn_2]$	-0.68	-1.85	f
Cp^*_2Mn	-0.96	-2.57	63a
$[Pn^*_2Co_2]$	-0.74	-2.75	f
Cp^*_2Co	-1.91		74
Cp_2Co	-1.31^e	-2.28^d	73, 74
$[Pn^*_2Ni_2]$	-0.82	-2.52	f
Cp^*_2Ni	-1.05^d		33
Cp_2Ni	-0.49^d	$-2.06^{b,d}$	73

[a] Experimental reduction potentials for compounds **1**−**5** determined using square-wave voltammetry in THF containing 0.1 M $[^nBu_4N][BF_4]$. [b] Irreversible. [c] Corrected using $E° = 0.56$ V for Cp_2Fe^+/Cp_2Fe vs SCE in THF/$[^nBu_4N][PF_6]$. [d] Corrected using $E° = 0.40$ V for Cp_2Fe^+/Cp_2Fe vs SCE in MeCN/$[^nBu_4N][PF_6]$. [e] $E° = 0.51$ V for Cp_2Fe^+/Cp_2Fe vs SCE in glyme/$[^nBu_4N][PF_6]$. [f] This work.

in the following general behavior reported for the other complexes studied). In all cases for both systems, a stable voltammetric response was observed in terms of both the peak currents and peak potentials recorded, thereby indicating that the species produced upon oxidation or reduction of the complexes are electrochemically stable and do not undergo any follow-up homogeneous chemistry (i.e., chemical decomposition) after the heterogeneous electron transfer has occurred.

The potential scan rate was varied from 100 to 1000 mV s^{-1} for each of the systems I and II for each $[Pn^*_2M_2]$ complex. Figure 16 shows the resulting voltammetry recorded for **5** over system I, and the behavior of the other complexes is shown in the Supporting Information. In this and all other cases, the peak-to-peak separation was found to gradually increase with increasing scan rate, again consistent with each system exhibiting quasi-reversible electron-transfer kinetics. A plot of peak current versus the square root of the potential scan rate was linear, indicating in all cases that the voltammetry of systems I and II can be attributed to the diffusion of a species in solution and that neither the neutral species nor the products of either oxidation or reduction in systems I and II, respectively, are adsorbed onto the electrode surface.

In the case of **5**, an additional one-electron quasi-reversible oxidation is observed that is not seen for any of the other compounds **1**−**4**; it has a midpeak potential of +1.10 V (vs Ag) and is labeled as system III in Figure 17. Reversal of the scan direction after the oxidation peak of system III revealed the corresponding reduction peak, which is convoluted with an additional irreversible reduction peak at a slightly less positive potential than that of the reduction peak of system III (observed as an ill-defined shoulder on the reduction peak of system III in Figure 17). At larger scan rates, the irreversible reduction wave becomes more pronounced because of the larger shift in peak potential for an irreversible system than for the quasi-reversible reduction corresponding to system III. Clearly, some follow-up chemistry occurs after the oxidation of the $[Pn^*_2Ni_2]^+$ complex to form the $[Pn^*_2Ni_2]^{2+}$ species, but an investigation to determine the likely species involved and the mechanism of any follow-up chemistry was beyond the scope of this paper and is a subject for future work. Repetitive potential cycling over system III revealed that the voltammetric responses for
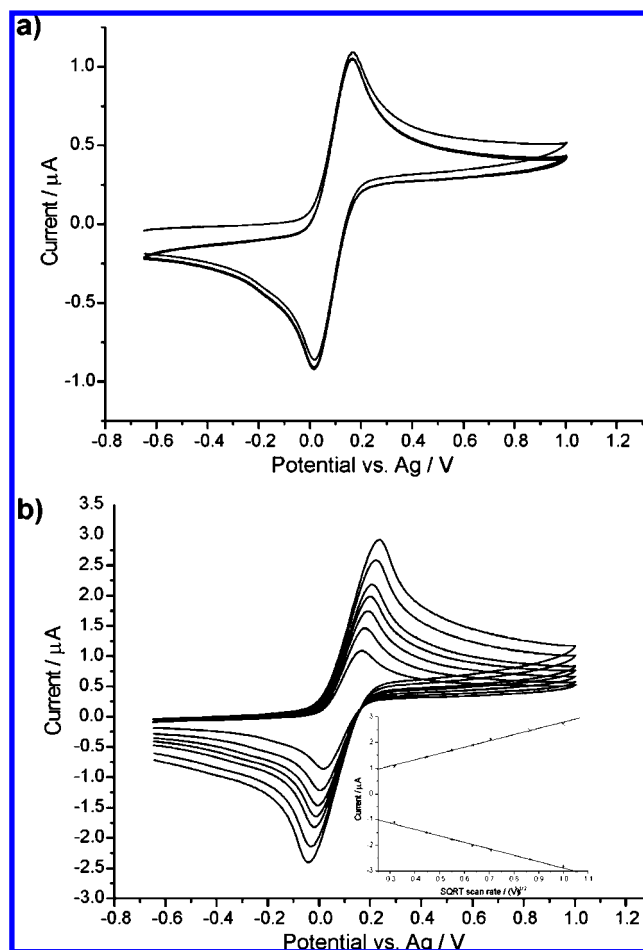

Figure 16. (a) Overlaid cyclic voltammograms (20 cycles) obtained by scanning over the region of system I for 1.1 mM **5** in THF containing 0.1 M $[^nBu_4N][BF_4]$. The scan rate was 100 mV s^{-1}. (b) Overlaid cyclic voltammograms of 1.0 mM **5** obtained by scanning over system I at varying scan rates (100, 200, 300, 400, 500, 750, and 1000 mV s^{-1}). Inset: corresponding plots of the reductive and oxidative peak currents vs the square root of the scan rate.

both the oxidative and reductive waves are stable, as was the case with systems I and II, while varying the voltage scan rate again revealed that the voltammetry was under diffusion control and that no fouling or adsorption onto the electrode surface was occurring.

Cyclic voltammetry experiments on **1** gave results that differed markedly from those for the other complexes studied, as shown in the Supporting Information. Upon a first scan from 0.00 to +1.00 V (vs Ag), an oxidative peak was observed at +0.73 V. However, upon reversal of the scan direction, no corresponding reduction peak was observed, indicating that this process is electrochemically irreversible. Upon continuation of the scan in the reductive direction, a reduction wave with a corresponding oxidation wave centered on a midpeak potential of −1.66 V was observed. In addition, 20 repeat cycles were recorded separately over the regions of system I and II, and the potential scan rate was varied over each system. For both systems, the observed voltammetry was again characteristic of diffusion-controlled behavior. Furthermore, despite the electrochemical irreversibility of system I, the voltammetric response remained stable over many repeat scans, indicating that the product formed is not fouling the electrode surface or reacting with the parent neutral $Pn^*_2V_2$ species. The absence of a stable monocation for **1** may be attributed to the possible rearrange-
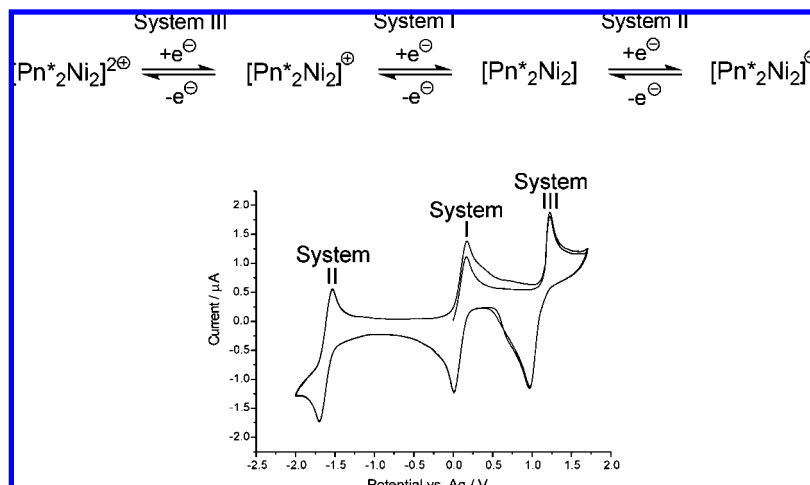
Figure 17. Full survey scan for **5** (1.1 mM), clearly showing three quasi-reversible electrochemical processes in the potential window.

ment of the Pn* ligand to an η^8-Pn*V(III) moiety upon oxidation; indeed the isolation of a number of (η^8-pentalene)V(III) complexes has been documented by Jonas et al.[70]

In order to rigorously ascertain the number of electrons transferred in each redox process associated with systems I and II for each [Pn*$_2$M$_2$] complex, chronoamperometry using a platinum microelectrode in a two-electrode configuration was employed. A potential step was applied from a potential at which no current is observed to a potential past the oxidative or reductive peak for system I or II, respectively. The current transients (i) were then fitted using the empirical procedure of Shoup and Szabo,[71] which describes the current transient at a microelectrode on both short ($\tau < 1$) and long ($\tau > 1$) timescales according to eq 3:

$$i = 4nFC^*Drf(\tau) \qquad (3)$$

in which n is the number of electrons transferred, F is the Faraday constant (96 485 C mol^{-1}), C^* is the bulk concentration (mM), D is the diffusion coefficient (m^2 s^{-1}), r is the radius of the electrode (m), and $f(\tau)$ is given by

$$f(\tau) = 0.7854 + 0.8863\tau^{-1/2} + 0.2146\exp(-0.7823\tau^{-1/2})$$

where $\tau \equiv 4Dt/r^2$ is a dimensionless time related to the actual time t (s). The Shoup–Szabo best fit simultaneously gives optimized parameters for D and nC^*. As C^* is known, the other parameters can then be deduced.[69]

Reassuringly, the diffusion coefficients reported herein for all of the neutral complexes **1**–**5** studied in this work are all reasonably similar, with values of $(7.0 \pm 1.0) \times 10^{-6}$ cm^2 s^{-1}, as is expected for complexes of almost constant size. Furthermore, they are all in excellent agreement with the D value of 8.0×10^{-6} cm^2 s^{-1} estimated using the Wilke–Chang approximation,[72] given by eq 4:

$$D = 7.4 \times 10^{-8}\frac{T\sqrt{m\chi}}{\mu V^{0.6}} \qquad (4)$$

where T is the temperature (K), m is the molar mass of the

solvent (g mol^{-1}), χ and μ are the solvent association parameter and the viscosity (cP), respectively, and V is the molar volume of the solute at its melting point (cm^3 mol^{-1}). Furthermore, the Shoup–Szabo analysis confirmed that systems I and II for compounds **1**–**5** are all quasi-reversible one-electron redox processes, a result that can be rationalized in terms of the generalized scheme shown in Figure 15.

Table 4 summarizes the electrochemical data for compounds **1**–**5** and, for comparative purposes, also includes literature data for the corresponding one-electron redox processes observed for selected metallocene compounds. First, it should be noted that the first one-electron oxidation for each member of the Pn* series is at a more anodic potential than that observed for the analogous mononuclear Cp or Cp* metallocene, with the sole exception of Cp$_2$Ni. This may be rationalized by the bonding description used for the syn-(μ:η^5,η^5)M$_2$ ligation mode of Pn*: formally, the bridgehead-bond π-electron pair is shared, and therefore, each five-membered ring cannot contribute as much electron density to each metal center as the Cp/Cp* ligands can; thus, the metals are less electron-rich. Nonetheless, a trend toward more-negative oxidative potentials is observed on traversing from V to Ni, which is consistent with the increasing population of higher-energy antibonding orbitals and corresponds well with the MO scheme for these compounds (Figure 13). In contrast, the reductive processes follow a different trend, with an increase in $E°$ values in going from **1**–**3** followed by a sharp decrease for **4** and **5**; this correlates qualitatively with the energies of the LUMOs (for **3**, the LUMO is the lowest-energy SOMO) shown in Figure 13.

For **5**, a further single-electron oxidation wave is now observable. For symmetrically bridged bimetallic complexes showing reversible electrochemical events, the separation between the first and second oxidation or reduction permits the comproportionation constant, K_c, which is a measure of the degree of interaction between the metal centers, to be calculated using eq 5:

$$K_c = \exp\left[(E_1° - E_2°)F/RT\right] \qquad (5)$$

where $E_1°$ and $E_2°$ are the corresponding values for the first and second reduction potentials respectively. In the present case of **5**, K_c is the equilibrium constant for the reaction

$$[\text{Pn*}_2\text{Ni}_2]^{2+} + [\text{Pn*}_2\text{Ni}_2]^0 \rightarrow 2[\text{Pn*}_2\text{Ni}_2]^+$$

The peak separation of 1.01 V gives a K_c value of 1.2×10^{17};

(70) Jonas, K.; Gabor, B.; Mynott, R.; Angermund, K.; Heinemann, O.; Kruger, C. *Angew. Chem., Int. Ed. Engl.* **1997**, *36*, 1712–1714.
(71) Shoup, D.; Szabo, A. *J. Electroanal. Chem. Interfacial Electrochem.* **1982**, *140*, 237–245.
(72) Wilke, C. R.; Chang, P. *AIChE J.* **1955**, *1*, 264–270.
(73) Holloway, J. D. L.; Geiger, W. E., Jr. *J. Am. Chem. Soc.* **1979**, *101*, 2038–2044.
(74) Connelly, N. G.; Geiger, W. E. *Chem. Rev.* **1996**, *96*, 877–910.

values in excess of 10^6 are considered to denote extensive delocalization, so 5^+ belongs to a class-III system in the Robin−Day scheme.[75] Compound **5** exhibits a K_c that is several orders of magnitude larger than those for other pentalene complexes, such as $(Cp*M)_2Pn$ (M = Fe, Co, Ni, Ru; $K_c = 10^4-10^{14}$)[76] and $[Mn(CO)_3]_2Pn$ ($K_c = 10^6$).[77]

Conclusion

This work has demonstrated that the permethylpentalene ligand can stabilize bimetallic arrangements for the first-row transition metals V, Cr, Mn, Co, and Ni. The metals are held in very close proximity, and their internuclear interactions are a classic interplay of atomic size and electron count. As we had hoped, $Pn*_2M_2$ complexes display a rich variety of magnetic, electronic, and redox behaviors. The $[Pn*_2M_2]^+$ and $[Pn*_2M_2]^-$ derivatives are formally mixed-valent and are currently under investigation.

Supporting Information Available: Solid-state magnetic susceptibility data for **3** and a CIF file and cyclic voltammetry data for compounds **1**−**5**. This material is available free of charge via the Internet at http://pubs.acs.org.

JA8057138

(75) Robin, M. B.; Day, P. *Adv. Inorg. Chem. Radiochem.* **1967**, *10*, 247.
(76) Manriquez, J. M.; Ward, M. D.; Reiff, W. M.; Calabrese, J. C.; Jones, N. L.; Carroll, P. J.; Bunel, E. E.; Miller, J. S. *J. Am. Chem. Soc.* **1995**, *117*, 6182–6193.
(77) Jones, S. C.; Hascall, T.; Barlow, S.; O'Hare, D. *J. Am. Chem. Soc.* **2002**, *124*, 11610–11611.